CHAPTER 5—APPLYING LISA

5.1 Getting Started

5.1.1 General

By definition, a Level I stability analysis is a broad, multiproject analysis intended to support planning-level decision making (Prellwitz 1985a). A Level I analysis will generally be performed for relatively large landforms using information gathered primarily from soils, geology, and other resource inventories, air photo interpretations, the scientific literature, and the user's knowledge of a particular area. Some field verification of input values and distributions used, and of the LISA results by comparison to the locations, numbers, and sizes of actual failures on this or similar landforms, should be made. The reliability of the analysis should be qualitatively assessed by reporting the source of the input data and the amount of field verification that was done.

When first using LISA, it is instructive to use the program on areas for which field information is available and the failure potential is fairly well known and understood. This should include both stable aand unstable areas. This will give the first-time user practice in developing input distributions for a well-known area, a feeling for the range of probability of failure values to expect from LISA, and help in developing confidence in the analysis method and results.

Before running LISA for a particular study area, we recommend that the user perform sensitivity analyses using the DLISA program, which is described in part 2, chapter 4. Sensitivity analyses will aid the user in selecting ranges of input values that give the desired ranges in factors of safety and in identifying which variables are most important for that area. When possible, DLISA should be used to perform back-analyses on existing failures to estimate values for unknown variables—usually groundwater height, soil strength, and root strength.

5.1.2 Delineating Polygons

A polygon, as used in this manual, is a piece of ground for which PDF's for each input variable need to be estimated for a LISA analysis, and can vary in size depending on the scope of the analysis. We suggest that for preliminary analyses, the user start with available polygons for which there is existing information. Examples include the land type map units delineated in Land System Inventories (LSI) used in the Northern Region of the Forest Service, U. S. Department of Agriculture; soil units delineated in the Soil Resource Inventories (SRI's) used in the Pacific Northwest Region; and geologic units delineated in the Geologic Resources and Conditions (GRC) maps, also used in the Pacific Northwest Region.

If these polygons are deemed inadequate or inappropriate, polygons should be delineated based on bedrock and surficial geology, and geomorphic landform. Further refinement could be made based on slope, vegetative cover, and groundwater characteristics. A polygon might also be some area of interest, such as a harvest unit.

5.1.3 Using LISA for Level II Analyses

The infinite slope equation—thus, the LISA program itself—also may be applied to stability analyses for single projects; that is, an analysis of natural slopes or specific harvest units within timber sales that are anticipated (through a Level I analysis) to have stability problems. A stability analysis for project planning is, by definition, a Level II stability analysis (Prellwitz 1985a). The main difference between a Level I and Level II analysis of natural slopes is that typically a Level II analysis will have a greater quantity of field measurements and observations, and therefore a greater reliability in the results. The techniques discussed in section 5.3 also can be used to obtain the information for a Level II analysis.

One also could use the SARA (Stability Analysis for Road Access) program (Prellwitz and Hall 1992) to perform Level II natural slope analyses because it too performs a Monte Carlo simulation of the infinite slope equation. The intent of including the infinite slope equation in SARA is to allow users to analyze the stability of natural slopes along road locations prior to analyzing the stability of the road prism itself, because one would not want to locate a road on a slope that was inherently unstable. An advantage of using the SARA program for analysis of natural slopes away from road locations is that data files that are derived primarily from field observations and measurements (SARA data files) can be kept separate from data files derived primarily from inventory information (LISA files).

5.1.4 Data Files and Map Unit Subdirectories

There are three types of LISA data files—site, material, and groundwater. Site files contain the PDF's for ground slope, soil depth, root strength, and tree surcharge. Material files contain the PDF's for soil unit weight, friction angle, cohesion, and moisture content above the phreatic surface. The groundwater file contains only the PDF for groundwater–soil depth ratio. The data are broken into these three categories to facilitate the analysis of various site conditions with a single material type.

The data files are stored on computer disk in a subdirectory with an `.MPU` extension. We call this subdirectory a "map unit." A map unit is nothing more than a mechanism for grouping data files and can represent whatever is convenient for the user. For example, a map unit might represent a landtype map unit (from a Northern Region Land System Inventory), a planning analysis area, or a timber sale.

5.2 Selecting Input Distributions—General Comments and Helpful Hints

For analysis of large landforms, statistical distributions that represent the spatial distribution of the values for each parameter are required. For example, in a particular landform, we estimate that 40 percent of the land area has soil depths between 2 and 4 feet, and 60 percent of the land area has soils depths between 4 and 8 feet. This spatial distribution could be represented by a frequency histogram with two classes. In a Level I analysis, the goal is not to determine where those soils depths are located on a particular piece of ground; this more site-specific information is obtained during a Level II or III investigation.

If measurements are available for any variable, the distribution selected can be whatever shape best represents the data. An initial step in this modeling process consists of plotting a relative-frequency histogram of the data using *equal* class widths. As stated earlier, this relative-frequency histogram may be used directly in LISA, or another distribution that generally fits the shape of the frequency histogram may be used. One may feel more comfortable using actual data in the form of a histogram. However, another sample set likely would have different frequencies. Also, unless the sample is large (more than 30 data values), it may not characterize actual field spatial variability, and use of a general statistical model may be more appropriate. Selection of a model can be done by visual comparison of the histogram of the data to a distribution shape plotted with the **Plot** option in LISA. With more than 30 data values, statistical tests for goodness-of-fit (such as the Chi-squared, K-S, or maximum likelihood) to the selected distribution can be performed. Benjamin and Cornell (1970) describe these techniques in section 4 of their chapter 4.

As mentioned in sections 2.2.1 and 2.2.2, when you have few or no data, then information from resource inventories (LSI, SRI, or GRC), slope maps, and air photos can be used to estimate a realistic range of values (a uniform distribution) or a range and most likely value (a triangular distribution) for some variables. We also discussed in section 2.2.3 a method for estimating the values for the mean and standard deviation for a normal distribution given a range of values.

Keep in mind that resource inventories usually are based heavily on air photo interpretation with limited field checking. The level of mapping is such that inclusions of other contrasting mapping units may exist in any mapping unit. The Clearwater National Forest LSI states that these inclusions may make up 15 percent of the land area in any given mapping unit (Wilson and others 1983). Therefore, when using soil depths or slope ranges, or estimating values for shear strength parameters based on the soil type given for a mapping unit, it may be advisable to extend the range of values beyond what is given. For example, one might use a histogram with three classes: one class with 85 percent of the values in the range given for the mapping unit, and two classes, each containing 7.5 percent of the values, with ranges greater than and less than the given range. Also, keep in mind that ranges given for SRI and LSI map units generally apply to the whole Forest. These ranges could be modified by air photo interpretation or by limited field sampling within the area being analyzed.

There is a natural but incorrect tendency to select a single value for a variable in the absence of field data. Single values imply certainty and no variability, which is unlikely. When you have no field data, your uncertainty is greatest, and the uniform distribution, which generally has the highest variance for a given range of numbers, is probably most appropriate.

A few general comments should be made regarding the normal and triangular distributions. The normal (or Gaussian) distribution is probably the most widely used distribution in probability and statistics. It typically is used to describe a process in which values are scattered about one "true" value such as would be observed in repeated laboratory experiments on a single specimen. It is quite natural to think of variability of a natural factor as being symmetrical about the mean value, and therefore the tendency might be to select a normal, or a symmetrical triangular or beta distribution. But keep in mind that when describing the spatial distribution of a variable such as soil depth or slope, there is no reason that it has to be symmetrical about a central value, and asymmetrical distributions should be given serious consideration.

There are a few other things to keep in mind when using the triangular distribution. As mentioned in section 2.2.2, the probability of a value occurring close to the minimum or maximum value is small. Therefore, you should use a slightly wider range of values than you would for a uniform or a histogram distribution, as illustrated in figure 5.1.

Also, the triangular distribution may poorly represent highly skewed or gapped data, in that more values will be simulated in the intermediate range than occur in the data, as illustrated by figure 5.2. There are two schools of thought here. You might assume that, if you had more data, the triangle would "fill in," and the triangular distribution is appropriate. Or you might decide to model your data as closely as possible by using a relative-frequency histogram or a lognormal with a fairly large coefficient of variation.

In summary, the particular distribution you select to model the estimated values of data is largely a matter of personal preference and judgment based on

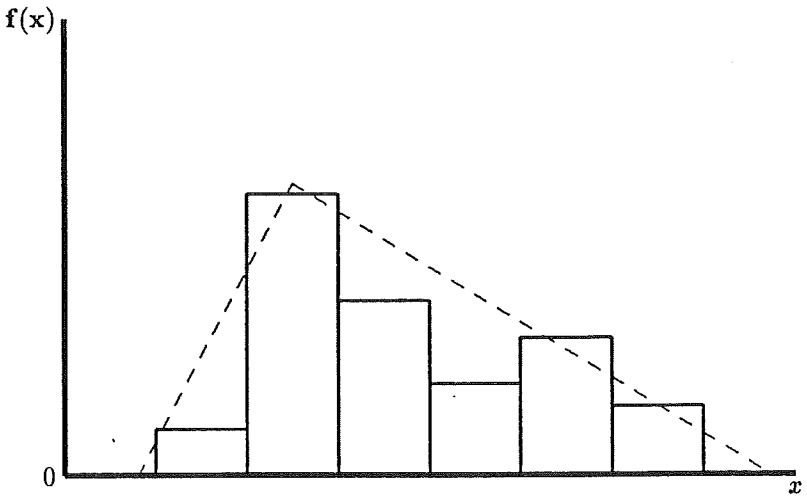

Figure 5.1—Extend the range of a triangular distribution compared to a uniform or histogram distribution.

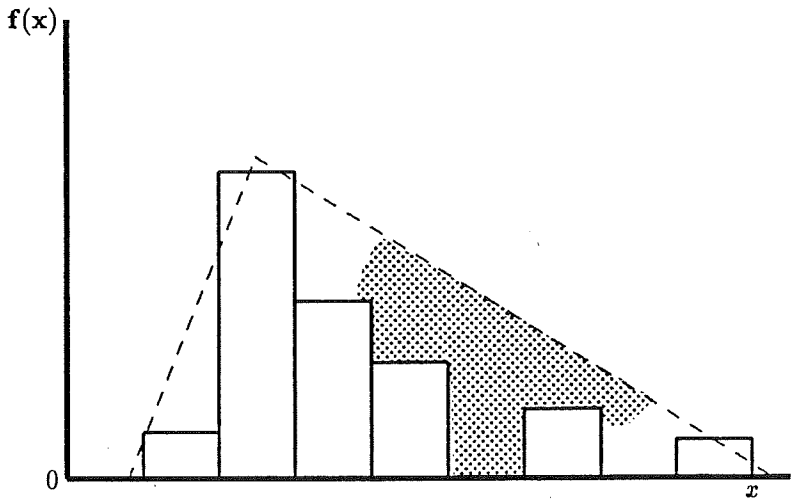

Figure 5.2—Triangular distribution may not represent highly skewed data well by oversampling values in the intermediate (▒) range.

your information and experience. *We strongly suggest that when more than one distribution is reasonable, or suggested by your information, you perform several simulations with each distribution and report the range of probabilities of failure obtained.*

5.3 Estimating Input Values and Selecting Distributions for Each Variable

Although the primary sources of information for developing distributions for a Level I stability analysis are resource inventories, geologic/soils maps, air photo interpretations, the scientific literature, and the user's experience and knowledge of a particular area, some data collection for verification of distributions

is recommended to lend credence to LISA results. *If field observations are to be made, at least 30 observations are needed to reasonably estimate the probability distribution of a given variable, although 10 to 12 observations could suffice if the user has field experience or knowledge of the variable.* This section is intended to provide guidance on data collection for slope, soil depth, and tree surcharge. In addition, possible values and distributions are discussed for tree surcharge, soil shear strength, tree root strength, and groundwater height, based on literature reviews.

5.3.1 Ground Slope

Within each polygon, slope measurements can be obtained from topographic maps. To avoid bias and to obtain a representative sample, it is recommended that a stratified random sampling scheme be used whereby a regular grid of cells is laid out over the polygon and a random location is selected within each grid cell. The ideal number of cells would be about 30 to 60, but 10 to 15 may suffice. At each location, the slope is calculated by using the map scale and contour interval. The slope values then are displayed in a histogram plot to assist the user in selecting an appropriate probability distribution to model the slope. Figure 5.3 illustrates a possible sampling grid. For smaller polygons, 30 to 60—even 10—cells may be impractical, requiring a different approach. In this case, measure a minimum, maximum, and most frequently occurring slope within the polygon to define a triangular distribution.

Through the use of digital elevation models (DEM's) or GIS (such as TIN in the ARC/INFO system), slope maps soon (or already) may be available. From these maps a histogram can be developed by measuring the percentage of the land area in the polygon that falls into various slope ranges (or classes).[6]

Because the factor of safety calculated with the infinite slope equation is quite sensitive to slope, some followup field measurements should be made. These measurements can be made using a hand-held inclinometer or Brunton compass and likely would be taken along roads or trails when the user is in the field gathering information on soil depth and vegetation cover.

Always keep in mind when making slope measurements that the surface slope is assumed to be parallel to the failure plane (commonly the soil-bedrock interface) in the infinite slope model. This assumption often is valid for some lateral extent, particularly in colluvial slopes. However, there may be field conditions where the ground surface is not parallel to the failure plane, such as with benched surface topography caused by glacial-fluvial or alluvial deposits over a planar bedrock surface. In this case, using the ground slope variations in LISA may be inappropriate; rather, estimates of the slope of the potential failure plane should be used. This slope might be observed in stream channels or by using an impact penetrometer (section 5.3.2). If rotational failures develop in the benches, using LISA with the conditions that exist at the center of gravity of the failure mass might be more appropriate (Prellwitz 1988).

5.3.2 Soil Depth

Soil depth does not necessarily mean the total thickness of unconsolidated material. It is common to apply the infinite slope model to conditions of a thin soil mantle overlying competent bedrock. In this case, soil depth is obviously the depth to bedrock. However, a translational failure plane may develop at any hydraulic conductivity contrast where positive pore water pressures can develop. Therefore, the depth to the failure plane may be much less than the depth to

[6]Information on existing digital elevation models can be obtained from: Western Mapping Center, National Cartographic Information Center, U.S. Geological Survey, 345 Middlefield Road, Menlo Park, CA 94025; phone (415) 329-4309, or FTS 459-4353.

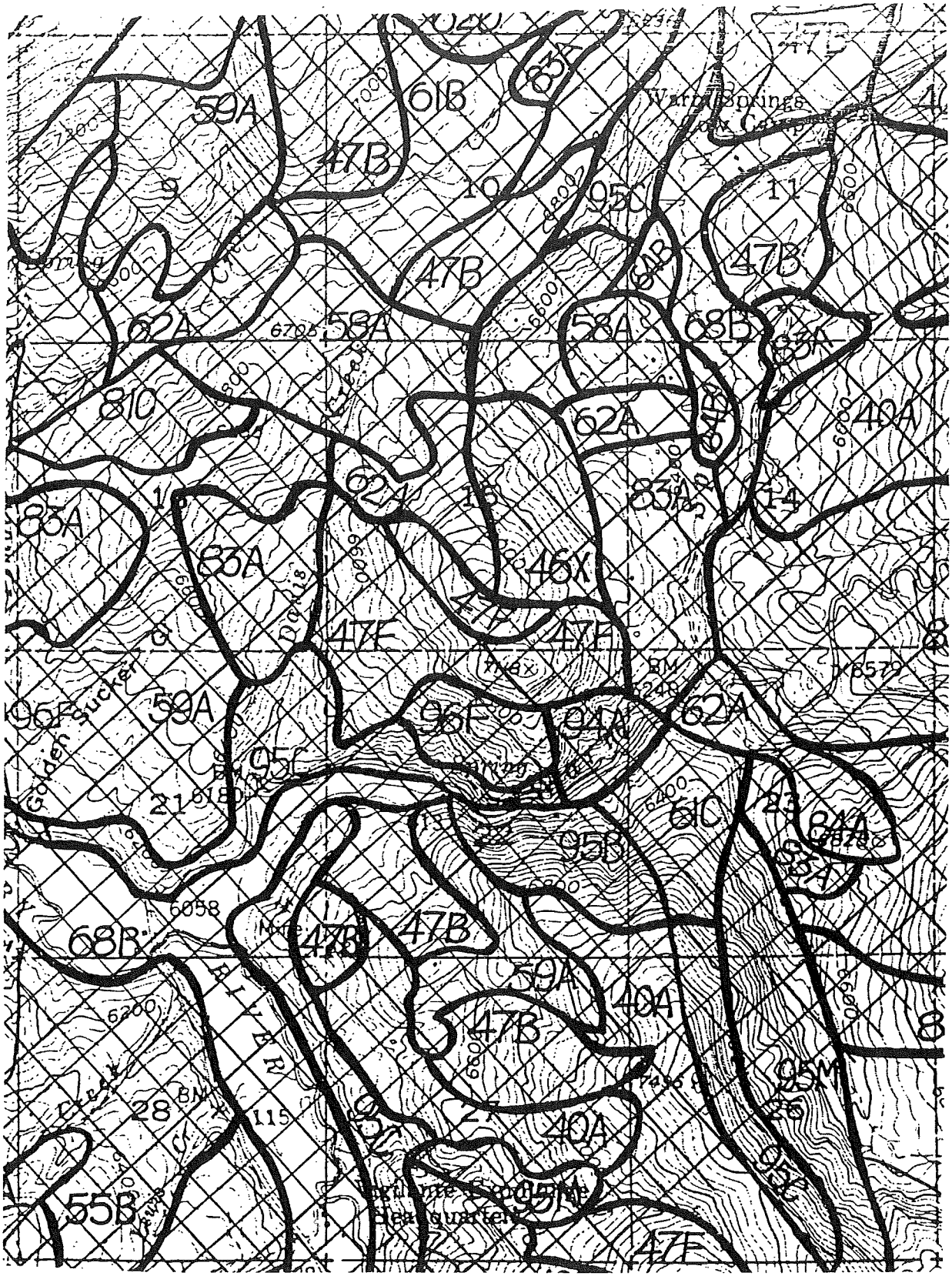

Figure 5.3—Stratified–random sampling grid for sampling ground slope.

competent bedrock. Examples of such conditions include loose near-surface soil in thick glacial or slope failure deposits, loose volcanics overlying denser soil layers, and loose colluvial soil overlying decomposed residual soil common in granitic terrane. *It is the depth to potential failure planes that should be described by the soil depth distribution.*

Initial estimates of the ranges in soil depth values usually can be obtained or inferred from resource inventories compiled by the forest soil scientist and geologist. The ranges then can be modeled with a uniform probability distribution. In most cases, some field measurements will be necessary to increase the reliability of the available soil depth information. Readily available locations for observing soil profiles include road cuts, ephemeral stream beds on valley side slopes, and root-throw pits formed at the base of blown-down trees. The latter two sources often will be accessible only on foot. If limited field reconnaissance is justified, then a hand-held, impact-driven soil penetrometer should be taken along to make as many soil depth soundings as time permits, ideally using a stratified random sampling scheme. When a stratified random sampling scheme is not feasible, then sampling can be done parallel to a road or along a given elevation contour or contours. In this situation, soil depth readings can be taken at regular intervals deemed appropriate by the investigator or at random locations within regular cells along the sampling trace.

Remember that the apparent soil depth measured as the slope distance along a cut face must be converted to vertical soil depth, as shown in figure 5.4. Seismic refraction is also a viable method for measuring soil depth. Also shown in figure 5.4 is the conversion for seismic refraction, which measures soil depth perpendicular to the refracting interface.

If bedrock cannot be observed or probed at a given sampling site, one can say that the soil is thicker than the observed soil depth. Likewise, if there are natural bedrock outcrops in the area, then the minimum soil depth should be considered negligible or nil. These observations, known as "soft data" or "inequality data," can help bracket the range of soil depths in a polygon.

5.3.3 Tree Surcharge

As stated in section 3.3, the factor of safety calculated by the infinite slope equation is fairly insensitive to the value of tree surcharge (q_0), particularly when soil depths are greater than 5 feet. Consequently, tree surcharge often is omitted from the infinite slope equation. When soil depths are less than 5 feet and especially when less than about 2 feet, the factor of safety may vary slightly with tree surcharge. Simons and others (1978) have shown that when $C_s + C_r < 62.4 D_w \tan\phi' \cos^2\alpha$, tree surcharge will have a positive effect on stability. Otherwise, tree surcharge will have a negative effect. Therefore, LISA includes tree surcharge so that its actual effect can be evaluated for any given set of field conditions.

Tree surcharge depends on the species, size, and density of the timber stand. Considering the weight to be uniformly distributed across the entire slope area is a common assumption for stability analysis (Greenway 1987; Sidle 1984a; Wu and others 1979). Estimates of equivalent uniform tree surcharge can be obtained from timber inventories of the volume of timber per acre and the weight per board foot of that timber. If the values given are for merchantable timber, they should be increased somewhat to account for the nonmerchantable volumes. The estimated range of tree surcharge values then can be modeled with a uniform distribution. An example calculation is shown below:

$$(3 \text{ to } 5 \text{ lb/bf}) \times (100{,}000 \text{ bf/acre}) \times (1 \text{ acre}/43{,}560 \text{ ft}^2) = 7 \text{ to } 12 \text{ psf}$$

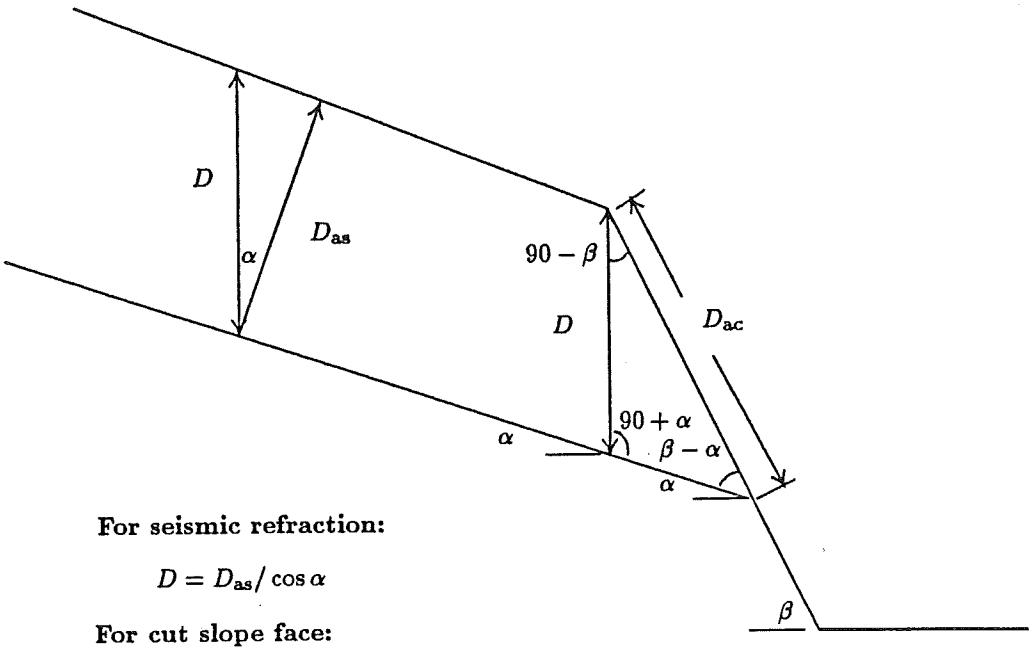

For seismic refraction:

$$D = D_{as}/\cos\alpha$$

For cut slope face:

from law of sines, $\frac{D}{\sin(\beta-\alpha)} = \frac{D_{ac}}{\sin(90+\alpha)}$:

$$D = \frac{D_{ac}\sin(\beta-\alpha)}{\sin(90+\alpha)}$$

Figure 5.4—Conversion of apparent soil depth measured along a cut slope face (D_{ac}) and apparent soil depth measured by seismic refraction (D_{as}) to vertical soil depth (D).

Gray and Leiser (1982) discussed a slightly different method for calculating tree surcharge. They considered a Douglas-fir stand in the Cascade Range of central Oregon that contained 50,000 to 65,000 board feet of merchantable timber per acre. At 10 lb/bf, the uniform surcharge would be 12 to 15 psf. If the weight of the trees is divided by the actual basal area of the trees (300 to 500 ft^2/acre), the stress directly under a tree would be about 1,400 psf. They then assumed that the weight of the trees was distributed over 75-ft^2 circles spaced 30 feet apart in a cubic array. In this case, the 1,400 psf surface stress would produce a stress increase of 20 to 75 psf midway between trees at depths of 5 and 20 feet, respectively. They concluded that even with this more exact analysis method, tree surcharge plays an insignificant role in slope stability.

Without tree species and density data, estimates of tree surcharge can be taken from the literature. When doing so, care must be exercised to ascertain whether an equivalent uniform surcharge or a surcharge directly under the tree is being reported. An equivalent uniform surcharge is recommended because the stresses at depth and between trees will not be as high as the surcharge directly under the tree. Some equivalent uniform surcharge values from the literature are listed in table 5.1.

5.3.4 Root Strength

It is well documented that tree roots provide some shear strength to a soil mass (Gray and Leiser 1982; Greenway 1987). In a general sense, tree roots are thought to stabilize slopes in three ways:

Table 5.1—Tree surcharge values reported in the literature

	Species	q_0, psf
Greenway 1987	Unspecified, 30–80 m high	10–40
Sidle 1984a	Sitka spruce, Alaska	$N[52.5, 10.4]$
Wu and others 1979	Sitka spruce, 100 to 200 feet high	50

- By providing a laterally reinforcing surface layer that acts as a membrane to "hold the underlying soil in place" (O'Loughlin and Ziemer 1982).
- By anchoring an unstable soil mantle to stable subsoils or rock where the roots penetrate a potential failure surface.
- By acting as buttress piles or arch abutments or both to support the soil uphill from the trees (Gray and Megahan 1981).

Gray and Leiser (1982) suggested that roots reinforce soil by providing tensile resistance in a manner similar to the reinforcement provided by steel straps in mechanically stabilized earth-retaining structures, except that metal bars are much stiffer than roots. Gray and Ohashi (1983) found that soil reinforced with natural and artificial fibers exhibited larger peak shear strength in loose and dense sands and less postpeak reduction in shear strength in dense sand at high strains. They also found that fibers slipped and pulled out, which limited the strength increase to values much less than would be predicted by the tensile strength of the fibers alone. Gray and Ohashi (1983) and O'Loughlin and Ziemer (1982) found that fibers and roots did not affect the angle of internal friction of sand. Therefore, root strength can be thought of as supplemental cohesion that is added to the soil shear strength in the numerator of the infinite slope equation.

Some attempts have been made to quantify the magnitude of root reinforcement by measuring the tensile strength of individual roots, by direct shear tests on soil-root masses, by pull tests on large root systems or whole trees, and by back-analysis of existing failures. These methods are described in detail in appendix B. Measurements using each of these methods clearly show that root reinforcement increases with greater root density (area of roots per area of soil).

Several researchers have used the tensile strength of individual roots (T_r) in mathematical models to estimate the root resistance per unit soil area (t_R) (Gray and Leiser 1982; Gray and Ohashi 1983; Waldron 1977; Waldron and Dakessian 1981; Wu and others 1979). These models are all similar in that they resolve the tensile force that develops in the roots during shear (T_r) into a tangential component (T_s) that directly resists shear, and a normal component (T_n) that increases the confining stress on the shear plane, thereby increasing the frictional component of soil shear strength. Figure 5.5 illustrates the general model.

The models generally have two flaws:

- They do not consider that during a slope failure, not all roots will mobilize their maximum tensile resistance at the same time.
- Except for Gray and Ohashi (1983), they do not consider that roots may not mobilize their maximum tensile resistance because they may slip or pull out before they break in tension.

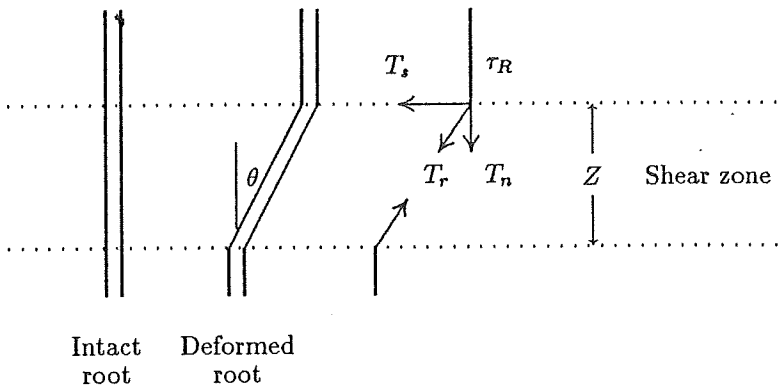

Figure 5.5—Fiber reinforcement model (after Gray and Ohashi 1983).

Additional research is necessary to increase our understanding of soil-root interaction during slope failure and to estimate defensible values for root strength to use in stability analysis. In the meantime, we suggest using root strength values reported in the literature, considering also root density and root distribution along the failure plane, as discussed in the next three sections.

5.3.4.1 Values of Root Strength Measured

Table 5.2 summarizes measurements of root strength per unit area of soil (t_R) made by several studies. Figure 5.6 shows a histogram created by stacking the ranges of values reported in each study. This histogram helps to visualize the most common measurements obtained by the studies. These values cover several species and a wide range of root densities.

5.3.4.2 Effect of Root Morphology and Suggested Probability Distributions

As discussed above, root strength depends not only on the tensile strength of the individual roots, but also on the pull-out resistance (or skin friction), and probably most importantly, on the morphology of the root system; that is, how many roots there are and whether they cross the failure plane. For example, western larch and black spruce have shallow root systems that spread laterally with small vertical sinker roots that penetrate deeper into the soil, while Douglas-fir has more ball-shaped root systems with a tap root that can penetrate deeply into the soil. Therefore, one might expect a greater potential root strength from Douglas-fir, particularly in deeper soils. Root tensile strength and morphology do not depend solely on the species of the tree. Within species, differences due to climate and site factors have been measured. Burroughs and Thomas (1977), for example, found that the roots of coastal Oregon Douglas-fir were twice as strong as the roots of central Idaho Douglas-fir. It is also known that the root systems of the same species can take on different shapes and strengths because of different slope, soil, and groundwater conditions. For example, uphill roots have been shown to be stronger than downhill roots, perhaps due to root tissue differences (Greenway 1987).

Use of the root strength values listed in table 5.2 requires some knowledge of root density and morphology at the site. Following the approach of Wooten (1988), we have adopted a soil-root classification scheme presented by Tsukamoto and Kusakabe (1984). This classification scheme attempts to account for the

Table 5.2—Root strength values reported in the literature

Investigator	Soil/vegetation type	Root strength, t_R	
		kPa	psf[1]
Endo and Tsuruta (1969a)[2]	cultivated nursery soil/1–2 m alder saplings[3]	1.6–11.5	33–240
Endo and Tsuruta (1969b)[4,5]	*Poa annua*, Ezo mugwort Ochada 0–5 cm depth	10.7–12.1	224–253
	(Bamboo) 5–20 cm depth	1.5– 4.9	31–102
Burroughs and Thomas (1977)[4]	Tyee S.S. (SM)/coastal Oregon Douglas-fir	11.5–22.7	240–474
	Idaho Batholith (SM)/ Douglas-fir	4.2–14.0	88–293
Wu and others (1979)[4]	SM ($\phi' = 35 - 37°$)/mixed Sitka spruce & hemlock	4.2– 5.5	88–115
Waldron and Dakessian (1981)[2,4]	clay loam/ponderosa pine seedlings	5.0	104
Ziemer (1981a)[2]	coastal sands/lodgepole[3]	0.2–17.3	4–362
O'Loughlin and others (1982)[2,6]	stony loam/beach	3.3	69
Waldron and others (1983)[2]	clay loam/5-year pine seedlings	3.7– 6.4	77–134
Riestenberg and	silty clay ($\phi' = 12°$) / sugar maples – head scarp	6.2– 7.0	130–146
Sovonick-Dunford (1983)[4]	– slip surface	3.8– 4.6	79– 96
	– average, entire slide	5.8	121
Wu (1984)[4]	SM ($\phi' = 30°$)/hemlock	5.6–12.6	117–263
	Sitka spruce	3.7– 7.0	77–146
	yellow cedar	5.4	113
Tsukamoto and Minematsu (1987)[7]	nursery loam/Sugi	1.8– 5.7	38–119

[1] 1 kPa = 20.9 psf
[2] Direct shear tests
[3] Measured over a wide range of root densities
[4] Tensile strength tests on individual roots
[5] Pull tests on roots
[6] Referred to by Sidle and others (1985) but not reviewed by these authors
[7] Isolated small trees and pulled—measuring basal shear resistance

differences in root morphology and density in relation to the location of the failure plane in estimating appropriate values for root strength. Figure 5.7 describes the four soil-root morphology types.

Figure 5.8 shows *suggested* PDF's for each soil-root morphology type for both densely forested and clearcut conditions. These PDF's were selected based on the following observations and assumptions:

- The measured values of root strength reported in the literature and summarized in table 5.2 and figure 5.6 were assumed to apply to densely forested types B and C, where roots intersect the entire failure plane. The mean and range of values are larger for type C to account for greater tree buttressing and root penetration along the base of the failure plane.
- The mean and range of values were reduced for types B and D based on three-dimensional modeling of failures as described in appendix C.
- All distributions have large standard deviations to account for the great variability and uncertainty in reported values.
- Lognormal probability distributions were selected to reflect the tendency for right skew in the data (fig. 5.6), thereby giving a low, but possible, probability of simulating relatively high values.

Appendix C discusses in greater detail the rationale for selecting the suggested PDF's for dense timber stands.

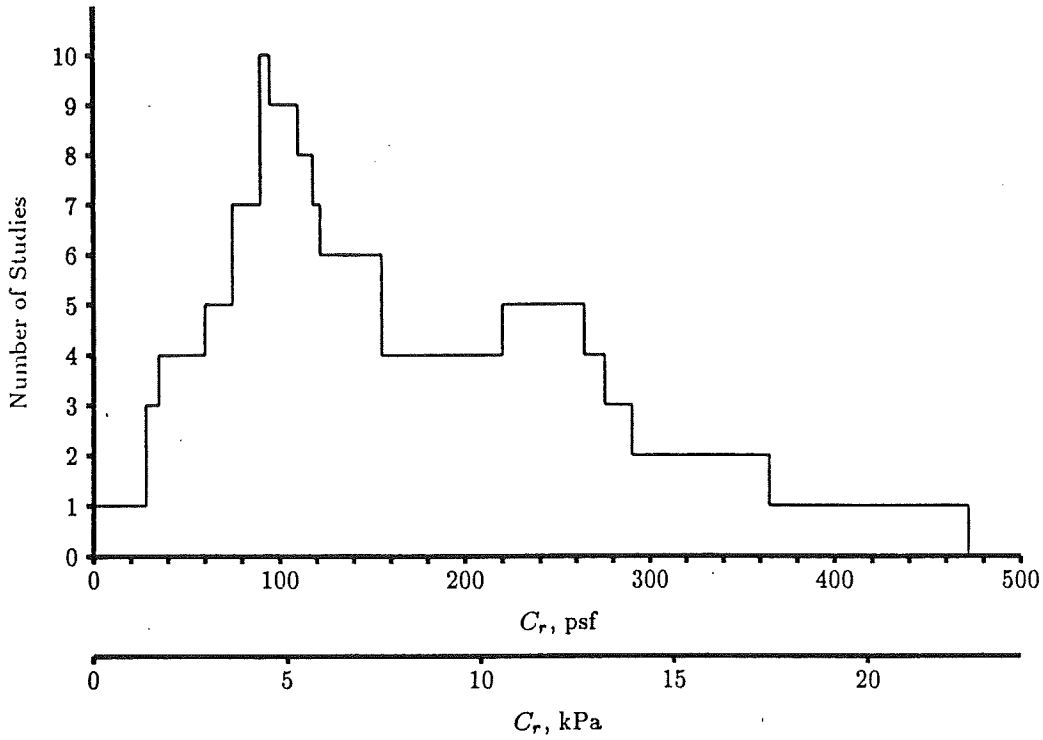

Figure 5.6—Root strength values given in 11 studies.

The user should adjust the suggested distributions to account for other factors such as roots in saturated clay (Waldron and Dakessian 1981), less dense timber stands, or the user's personal judgment and experience. We also suggest that the user talk to local soil scientists or silviculturists for their viewpoints as to which soil–root morphology type may apply in each polygon.

5.3.4.3 Effect of Timber Harvest on Root Strength

Much empirical evidence indicates that clearcutting increases the frequency of landslides, particularly debris avalanches on steep slopes with shallow soils. Gray and Leiser (1982), for example, cite 16 references that document this relationship. The primary reasons that tree removal causes instability are the resulting increase in groundwater height and the reduction of root strength. The increase in groundwater due to timber harvest is discussed in section 5.3.7.1.

After timber harvest, root decay causes both the numbers of roots and the tensile strength of the remaining individual roots to decrease with time (Burroughs and Thomas 1977). Ziemer (1981a, b) and O'Loughlin (1974) also measured a decrease in biomass and, consequently, root strength, with time after harvest using direct shear tests. These studies indicate that the period of minimum root strength is from about 3 to 5 years until about 10 to 20 years after harvest, depending on climate, which affects root decay and vegetation regrowth. In areas severely burned following harvest, minimum root strength may occur even sooner (0–3 years) (Prellwitz 1989). After about 10 to 20 years postharvest, root reinforcement will increase to its uncut level if significant regrowth has occurred.

Ziemer (1981a, b) estimated that, at its minimum, root reinforcement conceptually could be 20 to 40 percent of its undisturbed value (fig. 5.9). Therefore, we suggest using the distributions shown in figure 5.8 to represent the time of *minimum* root reinforcement after clearcut timber harvest for each soil-root morphology type. These distributions were obtained by finding a mean and standard deviation for a lognormal distribution which gives a mode value equal to about 30 percent of the mode for the uncut distribution.

If harvesting methods other than clearcutting are used, root strength may decrease less, and the distributions in figure 5.8 should be modified. Ziemer (1981b) discusses conceptual models for the change in relative root reinforcement following shelterwood and selection harvesting systems (fig. 5.9). A shelterwood system is described as having 70 percent of the original stand being harvested, followed by removal of the remaining trees 10 years later. For this system, Ziemer hypothesized the root reinforcement drops to about 70 percent of its uncut value at about 2 to 3 years postharvest, then rises to about 10 percent above the uncut value about 7 years after harvest as the residual trees quickly expand. About 5 years after the residual trees are harvested, root reinforcement again will drop to about 50 percent of the uncut value. The selection harvesting system is described at having 20 percent of the trees cut every 10 years. Ziemer anticipates that the root strength could decrease by about 3 percent 2 years after harvest, then increase to about 7 percent above the uncut strength due to the rapid expansion of the roots of the remaining trees.

5.3.5 Soil Shear Strength and Unit Weight

Little or no shear strength testing will be performed for a Level I investigation. When there are few shear strength data available for a soil from past Level II or Level III investigations, shear strength values likely will be estimated from values reported in the geotechnical literature, or be inferred indirectly from other soil properties that are available, such as soil gradation and relative density, or plasticity. Either method will require that the soil be classified according to the Unified Soil Classification (USC) system (ASTM D-2487-85 and D-2488-84). Field verification of soil classifications can be obtained by visual inspections of the *in situ* soils when the investigator is in the field measuring soil depth or ground slope. In addition, estimates of soil cohesion (C'_s) and friction angle (ϕ') values are possible by conducting back-analyses of slope failures observed in the study area, if there are any. Using all the above methods, the range and shape of the probability distributions for C'_s and ϕ' can be estimated.

When estimating values and PDF's for soil shear strength, keep in mind that the soil at the failure plane may not have the same properties as the bulk of the overlying material. Examples of this situation include thin clay seams at the failure plane, or a frictional resistance between soil and schist or phyllite bedrock that is less than within the soil mass itself (Alexander 1989). Therefore, sampling or testing the upper soil material may give inappropriate values. If multiple soil layers exist, weighted average values for soil shear strength parameters may be used to account for the portion of the failure plane passing through each soil type (see section 3.2). However, this refinement may not be justified for a Level I analysis.

If the unit weight of the material overlying the failure plane is different from the unit weight of the material through which the failure plane passes, the unit weight of the overlying material should be used, as that will give a more accurate computed value for effective stress. Again, with multiple soil layers, a weighted average value could be used, although again it might not be justified for a Level I analysis, particularly since the infinite slope equation is insensitive to unit weight.

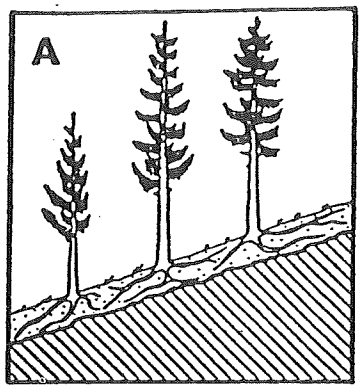

Type A—consists of shallow soils overlying fairly competent rock that roots cannot penetrate easily. The failure plane is mostly below the root zone, except where it intersects the ground surface. Because these roots are constrained by the bedrock, root densities may be greater than those for type D allowing for greater root reinforcement.

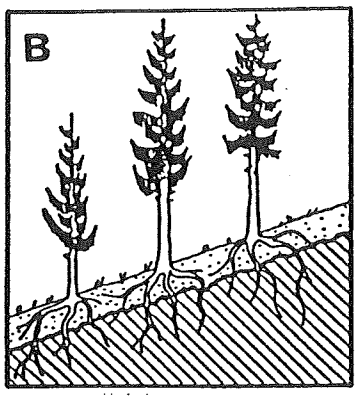

Type B—consists of shallow soils overlying fractured or weathered rock or compact glacial till that allows some root penetration. The amount of penetration depends on the number and nature of the discontinuities in the substratum; but in general the roots are restricted somewhat by the substratum. Root reinforcement is fairly significant because roots tend to intersect the failure plane along its full length.

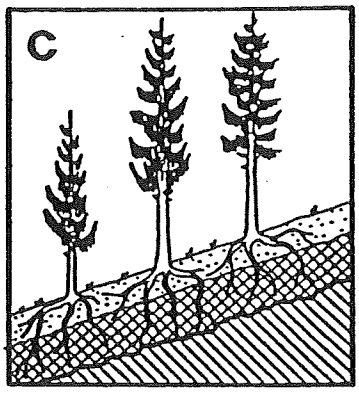

Type C—consists of a transition zone; that is, a nondistinct zone in which the soil shear strength and unit weight increase gradually with depth. It is assumed that the transition zone acts as a drainage barrier allowing the concentration of groundwater and the development of high pore-water pressure. As a result, the failure plane passes somewhere through the transition zone. It is assumed also that this zone is penetrated more easily by roots than is a less fractured substrate of type B. Therefore, the maximum root reinforcement is expected in type C. Examples of type C include decomposed granite over granite bedrock, and a loose ash or glacial till overlying a medium-dense compacted till over bedrock.

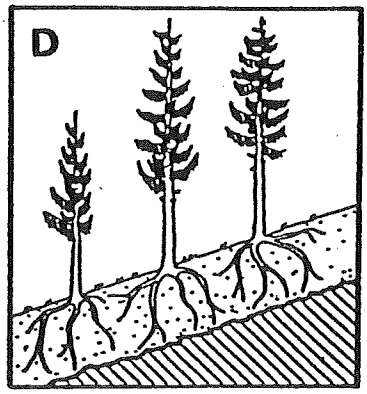

Type D—consists of soils and a potential failure plane both deeper than the root zone of the trees. The actual depth of the soil needed for a type D classification depends on the root morphology of the particular tree species. For example, less soil depth would be required for Sitka spruce, which has a shallow lateral root system, than for Douglas-fir, which has a deep root system. Because the bedrock does not constrain the root system, the root densities, and therefore the root strength, are assumed to be less than for those associated with type A.

Figure 5.7—Soil–root morphology types (after Tsukamoto and Kusakabe 1984).

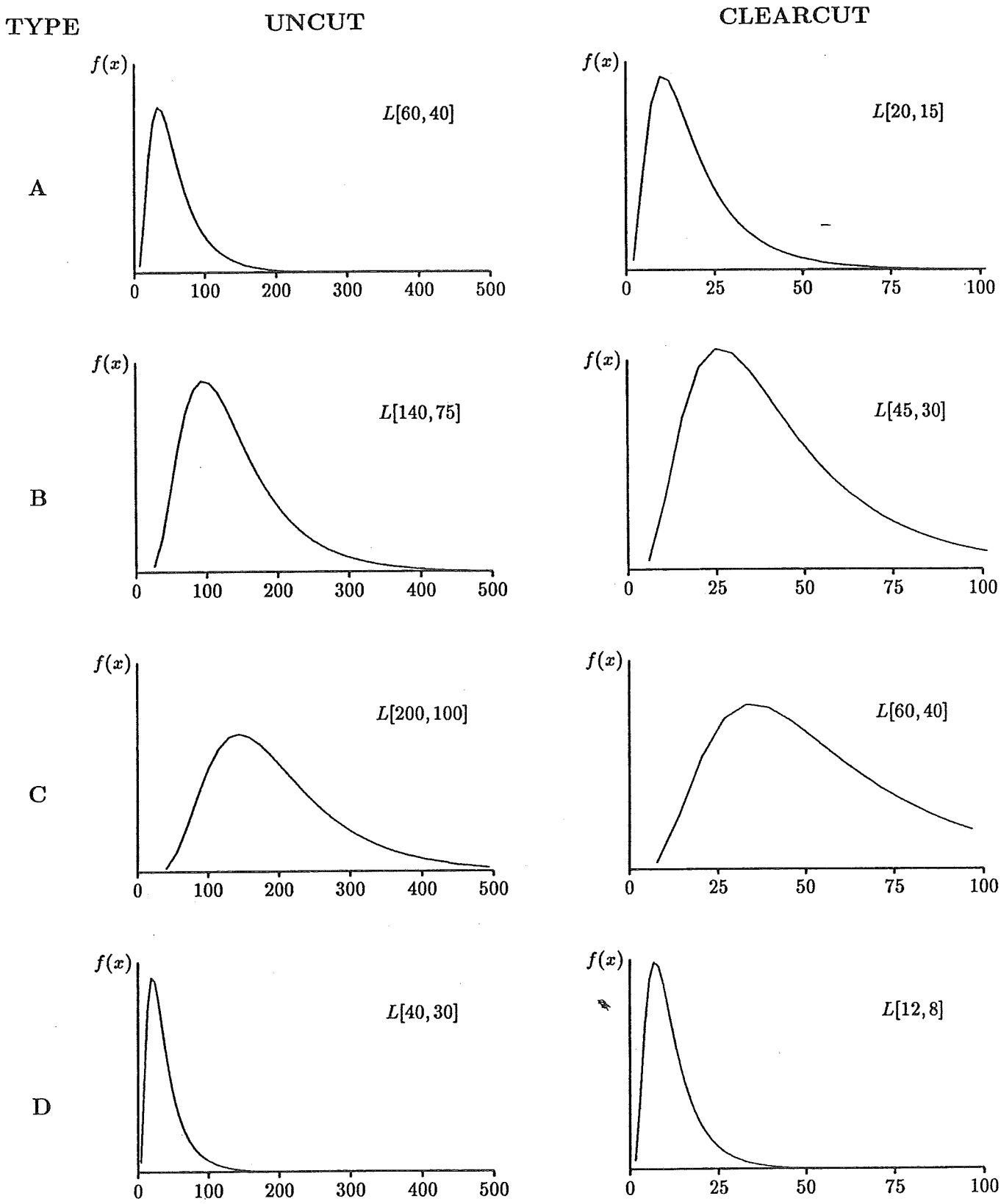

Figure 5.8—Suggested lognormal distributions describing possible ranges of C_r values for each soil–root morphology type in densely forested conditions, and during the 3– to 10–year period of minimum root strength after clearcut timber harvest.

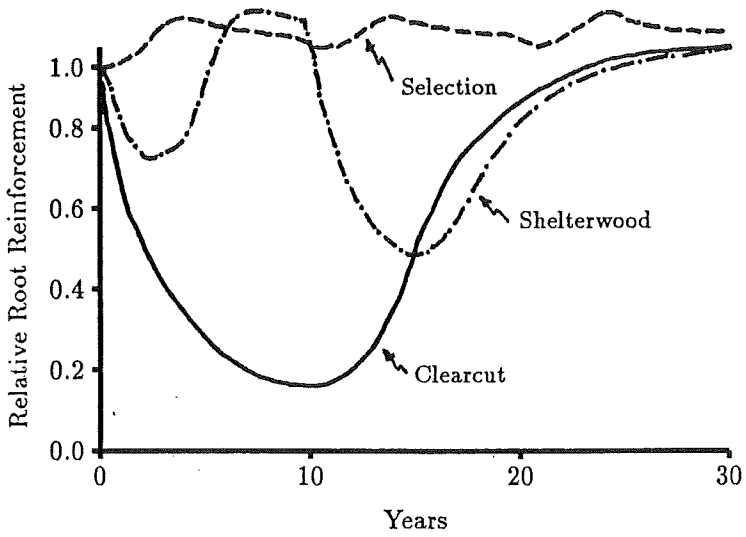

Figure 5.9—Changes in relative root reinforcement that occur after clearcut, selection, and shelterwood harvesting methods (after Ziemer 1981b).

The following subsections review shear behavior of sands, gravels, and clays, and discuss values and distributional shapes for C'_s, ϕ', and unit weight (γ_d) reported in the literature.

5.3.5.1 Distributions Reported in the Literature

Even nominally homogeneous soil is characterized by some spatial variation that must be described with a statistical model in a Level I analysis (Lumb 1975). However, the task of selecting appropriate PDF's for C'_s, ϕ', and γ_d is made difficult by other errors and uncertainties, namely:

- Uncertainty in the state of nature; that is, a lack of knowledge concerning the soil type that is actually within the polygon. This uncertainty can be reduced with extensive sampling.
- Random measurement errors, both in laboratory and in *in situ* tests.
- Systematic uncertainty in C'_s and ϕ' due to interpretations of laboratory test results. Some examples of interpretation differences are:
  - If one engineer arbitrarily defines failure in triaxial shear tests at 10 percent axial strain for a strain hardening soil, he or she would obtain lower values for friction angle than another engineer who defines failure at 15 percent axial strain.
  - If a linear regression is performed on four tests for cohesionless soils, a higher C'_s and lower ϕ' will commonly result than if C'_s was assumed to equal zero and the four resulting ϕ' averaged. This is true when the failure envelope is nonlinear.
  - With undrained triaxial shear tests, different C'_s and ϕ' values will be obtained depending on whether the maximum deviator stress or the maximum stress ratio is used as the failure criterion.
- Systematic conversion errors when predicting C'_s or ϕ' from *in situ* tests. For example, even if SPT blow counts are measured without error, there is still scatter in the relationships between blow count, relative density, and ϕ', which results in uncertainty in the estimates of ϕ'.

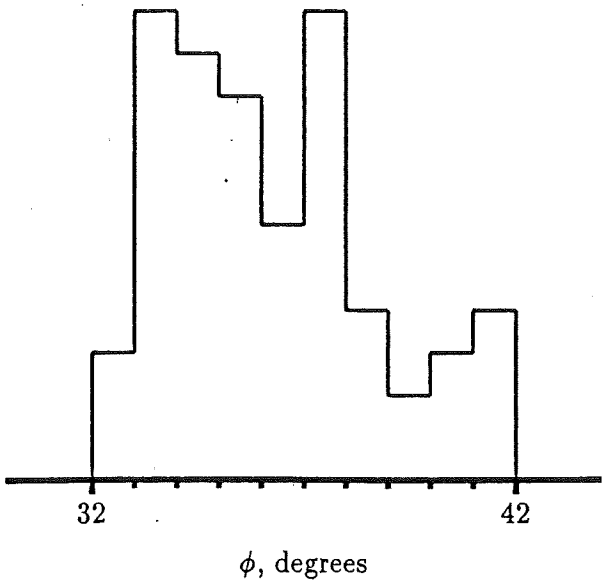

Figure 5.10—Histogram of ϕ' values reported by Schultz (1971) illustrating the limits and skewness of his data.

Variability and uncertainty in soil shear strength parameters have received a great deal of attention over the past 20 years as probabilistic methods in slope stability analysis have been studied. Early workers such as Lumb (1966, 1970) and Schultz (1971) recognized that the beta distribution best described the distribution of C_s' and ϕ' because observed values were limited in range and their distributions were asymmetrical (skewed). For example, figure 5.10 shows a histogram of ϕ' values reported by Schultz (1971). Although the distributions were asymmetrical, these early workers advocated using normal distributions because the mathematical rigor for calculating the probability of failure was greatly simplified. More recently authors have used (or recommended using) the beta distribution (Athanasiou-Grivas and Harrop-Williams 1979; Harr 1977; Oboni and Bourdeau 1983; Réthâti 1983) because with computers and simulation techniques the mathematical rigor is essentially avoided. Krahn and Fredlund (1983) used triangular distributions computing the limits from their sample data using:

$$\text{Minimum} = \bar{x} - 1.96s$$
$$\text{Maximum} = \bar{x} + 1.96s$$
$$\text{Apex} = \bar{x} - 3(\bar{x} - \text{median})$$

Other authors have reported coefficients of variation (c_v). A mean value for C_s' and ϕ' then can be multiplied by the c_v to obtain a reasonable estimate for the standard deviation. However, the shape of the distribution still must be selected. c_v and typical means and standard deviations for ϕ' as summarized by Harr (1977) are:

Soil	c_v	$\bar{x}$	s
GP	6.0%	36°	2.2°
GM, GW	5.3	37	2.0
SP, SW	5–15	35.6–40.5	2.8–5.3
SM	15.8	34.7	5.5

These large values of c_v apparently cover all relative densities and result in a wide range of ϕ' values. For example, if ϕ' of an SM soil was assumed to be normally distributed with a mean of 34.7° and a standard deviation of 5.5°, 95 percent of the values would lie between 23.7° and 45.7°, a range that effectively covers the observed range of sands. Therefore, these values have little practical usefulness. Lumb (1970) also provided some c_v values for comparison:

Soil	c_v for C'_s	c_v for ϕ'
Clay shale	95%	46%
Cohesive till	100	18
Residual sands and silts	17	6

These reported values of c_v *do* show that more variation in C'_s and ϕ' values typically can be expected for sands than for gravels, and much more variation can be expected in cohesive soils. Again, using these large values for c_v is probably not the best means to obtain PDF's for use in LISA. Rather, *we suggest that the user understand the shear behavior of sands and clays as discussed in the following sections, and then rely on the tables and figures presented there, along with knowledge of soil gradation, relative density, particle angularity, mineralogy, and* PI *to estimate shear strength values. These values then can be used to establish a probability distribution. We suggest using a uniform, triangular or relative-frequency histogram probability distribution when shear strength values are based on the tables and figures.* Although a beta distribution is more consistent with distributional shapes reported in the literature, the extra effort required to select P and Q values is probably not justified unless the user has some test data. Table 5.3 summarizes the information provided in sections 5.3.5.2 through 5.3.5.5 for estimating shear strength values.

5.3.5.2 Shear Strength of Sands and Gravels

The shear strength of sands and gravels results primarily from the frictional resistance of particle-to-particle contacts similar to those of a solid block sliding on a plane. Therefore, shear strength is directly related to the effective normal stress by the coefficient of friction, μ:

$$\tau = \sigma'_n \mu = \sigma'_n \tan \phi' \tag{5.1}$$

where τ is the shear strength, σ'_n is the effective normal stress, and ϕ' is the effective angle of internal friction (or friction angle). If soil cohesion exists, the equation for shear strength becomes:

$$\tau = C'_s + \sigma'_n \tan \phi' \tag{5.2}$$

where C'_s is the effective soil cohesion, which is the shear strength at zero normal force. Values for C'_s and ϕ' are measured in the laboratory using direct shear, triaxial compression, or (less commonly) ring shear testing devices (Bishop 1966; Bjerrum and Bjerrum 1960; Negussey and others 1988).

The angle of internal friction attributed to frictional resistance alone is called ϕ_μ. For quartz and feldspar, $\phi_\mu = 26°$ to 28° and for mica, $\phi_\mu = 7°$ to 23° (Horn and Deere 1962; Lee and Seed 1967). Sand, however, is not a solid block but an aggregate of interlocking particles. Additional energy is required to dilate, rearrange, or crush particles in order to shear the soil, which increases strength resulting in friction angles greater than ϕ_μ (Lee and Seed 1967; Rowe 1962, 1963).

Table 5.3—Summary of suggested values for C'_s and ϕ'

		Peak strength C'_s	Peak strength ϕ'_p	Residual strength C'_s	Residual strength ϕ'_r	Apparent cohesion
Silts, sands & gravels		0	From table 5.5, eq. 5.3, or fig. 5.11	0	Use table 5.5, eq. 5.3 or fig. 5.11 at $D_r = 0\%$	Depends on capillary suction and ϕ^b. Back-analysis commonly shows 20–60 psf for silty sands.
Clays	NC	0	From fig. 5.13	< 25% clay	0	Same as for sands and gravels.	
				> 25%– < 50% clay[1]	0	Use fig. 5.16 or 5.17 $\pm 3 - 5°$	Depends on capillary suction and ϕ^b. Values determined by back-analysis.
	OC	Depends on stress history. Typically 100–500 psf.	Depends on stress history. Heavily OC 25–40°. Lightly OC 20–30°, or use NC ϕ'_p.	> 50% clay	0	$10° - 24°$ for hydrous mica, $14° - 15°$ for kaolinites $9° - 15°$ for illite $4° - 10°$ for montmorillonites	

[1] Note, these may not classify as clays according to the USCS, but clay significantly affects the ϕ'_r value.

As the void ratio of sand decreases (unit weight increases) so does particle interlocking and, hence, friction angle.

Void ratio is most important in controlling the friction angle of sands. However, soil gradation, grain shape and roughness, grain size, and mineralogy also have some effect, with grain shape being most significant. The friction angles of angular soils tend to be greater than those of rounded soils, and those of well graded soils greater than those of poorly graded soils, because there is more particle interlocking. Mineralogy generally is considered to have little effect on the shear strength of sands and gravels. For instance, the ϕ_μ of mica is much less than the ϕ_μ of quartz, but highly micaceous sands have friction angles that are at most 1 or 2 degrees less than similar nonmicaceous soils when compared at the same unit weight or relative density (Hammond and Hardcastle 1987). However, mica can reduce the unit weight of soils, which indirectly causes lower friction angles.

It generally is assumed that, because of greater interlocking, coarse-grained soils have higher friction angles than do fine-grained soils when compared at a given relative density. This relationship can be seen in figure 5.11 and table 5.4, which give typical values of ϕ' for nonplastic silts, sands, and gravels. However, gradation and particle angularity generally play a more important role. For instance, one would expect poorly graded GM soils containing rounded gravels (such as soils originating from alluvial or glacial deposits) to have friction angles *less than* those of well graded SM soils containing angular fragments (such

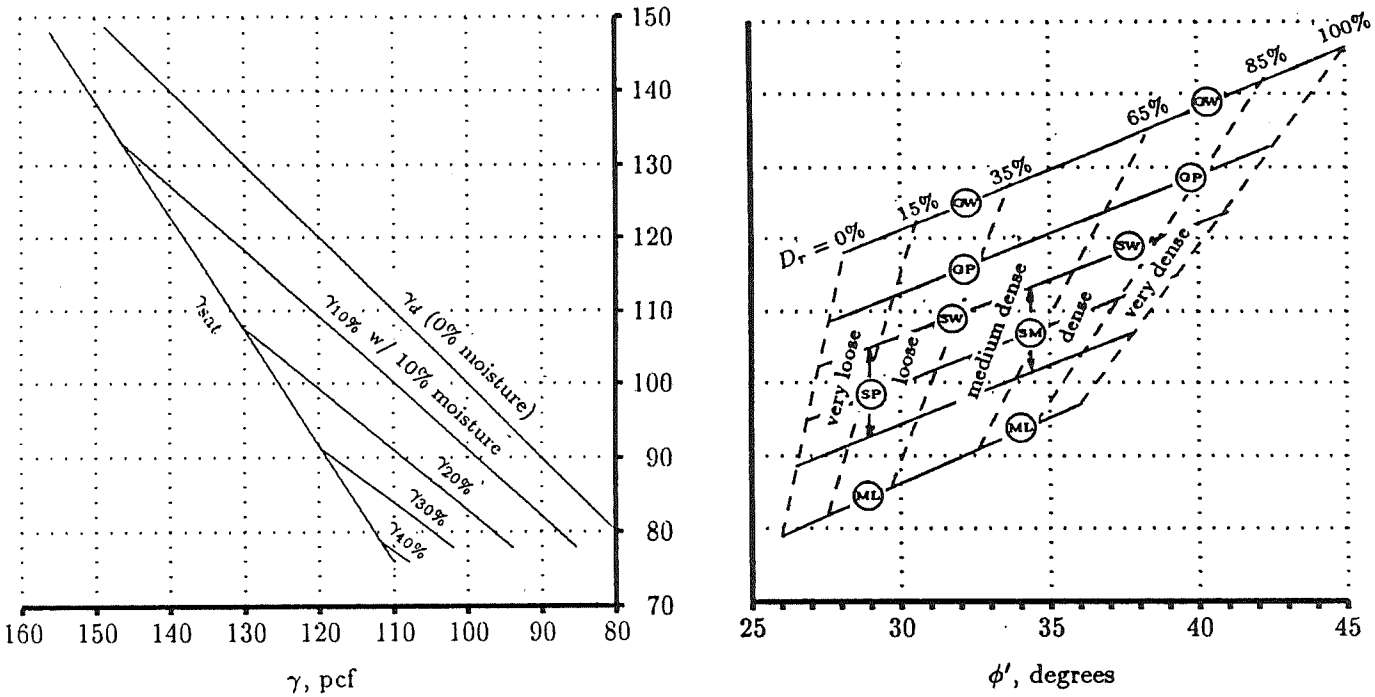

Figure 5.11—Relationship between D_r, and γ and ϕ' for nonplastic silts, sands, and gravels using $G_s = 2.68$ (after Prellwitz 1981 and U.S. Department of Navy 1974).

Table 5.4—ϕ' *vs.* D_r from Prellwitz (1981)

Soil type	ϕ'		$k_{\phi 1}$	$k_{\phi 2}$
	$D_r = 0\%$	$D_r = 100\%$		
GW	35°	45°	1.43	0.0043
GP, GM, or Coarse SW	33°	43°	1.54	0.0047
Med. SW, Coarse SP or SM	31°	41°	1.66	0.0051
Fine SW, Med. SP or SM	29°	39°	1.80	0.0057
Fine SP or SM	27°	37°	1.96	0.0064
ML	26°	36°	2.05	0.0067

as colluvial or residual soils) at the same relative density, which is contrary to the trend shown in figure 5.11 and table 5.4.

It also generally is assumed that gravelly sands would have higher friction angles than do sands containing no gravel. However, the effect of gravel on the shear strength of soils has not yet been explained fully in the literature. It is a difficult task to assess the effect of gravel on shear strength because it is difficult to sample and test specimens containing large particles. Conflicting test results are produced because the changes in gradation, void ratio, and limiting unit weights that occur when coarse fragments are added or removed make comparison of the shear strengths of fine and coarse soils uncertain. Several studies have shown an increase in friction angle as coarse sand and gravel are added to a soil when compared at the same relative density (D_r) (Holtz and Gibbs 1956; Wu and Baladi 1986). However, Holtz and Ellis (1961) and Siddiqi (1984) showed that adding gravel to fine soils had no effect on friction angles until the soils contained more than about 50 to 65 percent gravel. Siddiqi explains that with less than about 50 to 65 percent gravel (depending on the specific gravity of the soil particles), the gravels merely are floating in a matrix of finer soil, and shear strength is controlled by the fine soil alone. The gravel fragments do not contribute to strength until there is a high enough percentage that the fragments are in contact with each other.

Lambe and Whitman (1969) also note that large particles may lead to lower friction angles because large particles are able to roll more easily due to their centers of gravity being farther away from the plane of shear.

Also note that many studies cited in the literature have compared friction angles of fine and gravelly soils at the same void ratio rather than at the same D_r. Comparisons made on the basis of void ratio always show that the friction angles of sands are greater than those of gravels (Leslie 1963; Marachi and others 1969; Wu and Baladi 1986). This is because the addition of coarse fragments decreases void ratio but also increases the limiting unit weights. Therefore, at a given void ratio, a gravel soil will behave during shear as a looser soil (lower D_r) than a sand soil will, resulting in lower friction angles for the gravel.

5.3.5.2.1 Typical Strength Values and PDF's for C'_s and ϕ'—Typical values of ϕ' for nonplastic silts, sands, and gravels can be found in many textbooks (for example, Hough 1957; Lambe and Whitman 1969). Figure 5.11 and tables 5.4 and 5.5 can be used to obtain estimates of values for ϕ' and dry unit weight (γ_d) when no other information is available. Prellwitz (1981) comments that ϕ' values given by figure 5.11 appear conservative compared to data from

other literature. He developed a correlation equation for ϕ' to relative density (D_r) from these other sources:

$$\cot \phi' = k_{\phi 1} - k_{\phi 2} Dr \tag{5.3}$$

where $k_{\phi 1}$ and $k_{\phi 2}$ are coefficients given in table 5.4.

Estimates of D_r can be obtained using various penetration methods described by Prellwitz (1981) or by the portable density probe developed by Williamson on the Willamette National Forest (Williamson 1989).

Table 5.5 summarizes shear strength and γ_d values for cohesionless soils reported by several authors. This listing of C'_s, ϕ', and γ_d values is by no means exhaustive. The intent is to show the most likely values and the wide variety of values that can be obtained for any given soil classification. Table 5.5 is divided into three relative density classes—very loose to loose (D_r < 35 percent), medium dense (35 percent < D_r < 65 percent), and dense to very dense (D_r > 65 percent). In general, loose relative densities apply to volcanic ash, loess, and highly micaceous soils, and to the residual friction angle (ϕ'_r) for any soil (see section 5.3.5.4). Medium-dense relative densities apply to most residual and colluvial soils, and dense to very dense relative densities to compacted glacial tills and compacted fills. References 7 and 15 in table 5.5 correspond to equation 5.3 and figure 5.11, respectively. ϕ' values are peak values (ϕ'_p) unless otherwise noted.

Equation 5.3 and figure 5.11 (references 7 and 15 in table 5.5) represent data compiled from several sources, whereas the other references in table 5.5 are single studies. Equation 5.3 and figure 5.11 therefore cover a wider range of soil characteristics in terms of particle angularity, surface roughness, and mineralogy. Therefore, if you do not know much about a soil other than its USC classification, you might want to weigh equation 5.3 and figure 5.11 more heavily. If you do know more about the soil's characteristics, you might temper your estimate of ϕ' with values from other references. For instance, suppose you wish to estimate ϕ' values for a loose, medium- to coarse-grained SM with subrounded particles. Reference 7 indicates ϕ' in the range of 29° to 34°, and reference 15 indicates a range of 27° to 32.5°. Reference 17, however, shows ϕ' values of 27° to 28° for subrounded particles. This might suggest a triangular distribution with minimum, most likely, and maximum values of 26.5°, 27.5°, and 32.5°.

Nonplastic silts, sands, and gravels have no true cohesion (C'_s = 0). However, back-analyses of existing failures often yield C'_s values of 20 to 60 psf (<100 psf), particularly for silty cohesionless soils (Prellwitz 1989). Values of this magnitude in a uniform PDF would be appropriate for use in LISA in lieu of other information. This apparent cohesion may result from capillary suction (see section 5.3.5), or simply from differences between the actual failure mechanism and the assumptions of the infinite slope model.

Table 5.5 shows that several authors report large values for cohesion, up to 1,000 psf, in cohesionless sands and gravels (Holtz and Gibbs 1956; Schroeder and Alto 1983; Schroeder and Swanston 1987). This, of course, is not true cohesion but may result from the way in which laboratory test results are interpreted. Figure 5.12 illustrates that a cohesion intercept can result when a straight line Mohr's failure envelope is fit either to test data that are curved due to diminishing dilation with increasing effective stress, or to scattered test data that are due to test specimen variability or testing errors or both. The latter can result in either positive or negative intercepts. In either case, the positive C'_s and ϕ' values reported may be inappropriate for use in stability analysis at small effective stresses (shallow soil depths or steep slopes) because shear strength will

be overestimated. On the other hand, ignoring the cohesion intercept and using only the reported ϕ' value to compute shear strength could underestimate the actual shear strength at all confining stresses. This problem can be alleviated by performing shear tests only at effective stresses consistent with the *in situ* conditions or by modeling the Mohr's failure envelope as a curve with a power function (Miller and Borgman 1984). The power function option may be incorporated in future versions of LISA.

5.3.5.2.2 Typical Values for Unit Weight—Figure 5.11, tempered by values listed in table 5.5, can be used to estimate a uniform distribution for unit weight (γ_d). Figure 5.11 shows that γ_d for gravels is greater than γ_d for sands, which is greater than γ_d for silt. Also, angular soils tend to have lower γ_d than do rounded soils because angular particles tend to bridge and pack less efficiently (Wu and Baladi 1986).

In humid regions, soils may contain large amounts of organic matter that would give them unit weights much lower than those shown in figure 5.11. Alexander (1989) found that for inorganic soil horizons with more than 0.2 percent organic matter,

$$D_b = Ae^{-0.12OC^{1/2}} \tag{5.4}$$

where D_b is the bulk density of the −2mm fraction in Mgm^{-3}; A is 2.24 for loamy sands, 1.86 for sandy loams, and 1.73 for silts; and OC is organic carbon in gkg^{-1}. This equation had an r^2 of 0.850 and may not be applicable outside of southeastern Alaska where it was developed.

The dry unit weight in pcf can be estimated from D_b and the specific gravity of the soil particles (G_s) by

$$\gamma_d = \frac{D_b}{(\frac{D_b}{G_s \gamma_w} - 1)k + 1} \times 62.5 \frac{\mathrm{pcf}}{\mathrm{Mgm}^3} \tag{5.5}$$

where γ_w is the unit weight of water = 1 Mgm^{-3}, and k is the soil fraction greater than 2 mm by weight (Hammond and Hardcastle 1991).

5.3.5.3 Shear Strength and Unit Weight of Clays

In the stability analysis of natural slopes it generally will be correct to consider clays as $C'_s - \phi'$ soils and to perform an effective stress analysis. A total strength analysis (assuming $\phi' = 0$) is appropriate only for stability assessment of a saturated soil that is stressed quickly compared to the consolidation time of the soil, for example, when a clay slope is loaded or excavated quickly (Lambe and Whitman 1969).

5.3.5.3.1 Normally Consolidated Clays—The shear behavior of normally consolidated clays is similar to that of loose sands. Effective cohesion for normally consolidated clay is generally considered to be negligible (0–100 psf). Peak ϕ' (ϕ'_p) for normally consolidated clays has been found to decrease with increasing plasticity index, although there is much scatter in published data. Figure 5.13 shows a plot from Kenney (1959) illustrating this relationship. Bjerrum and Simons (1960) show a similar relationship. An equation for the line in figure 5.13 is:

$$\sin \phi'_p = 0.808 - 0.229 \log_{10} \mathrm{PI} \tag{5.6}$$

where ϕ'_p is the peak ϕ' for normally consolidated clay, and PI is the plasticity index in percentage. We suggest that the value from equation 5.6 ±5° or 6° be

Table 5.5—Reported values of γ_d, C'_s and ϕ' for silts, sands, and gravels

USC	% D_r	γ_d, pcf	C'_s, psf	ϕ', deg.	Source[1]	Material[2]
GW loose						
	0–35	*[3]	0	35–38	7	
	"	118–128	0	28–33.5	15	
	0	98–111	0	36.3–39.3	1	A, crushed
GW medium-dense						
	35–65	*	0	38–41	7	
	"	128–135	0	33.5–38.5	15	
	58	127	0	38.4–39	11	50% R–SR gravel
GW dense to very dense						
	65–100	*	0	41–45	7	
	"	135–145	0	38.5–45	15	
	"	125–135	0	> 38	16	
	*	119.5–137	0	39–46	6	SA–SR [alluvium]
	70	123–125.4	790-1140	38.0-41.4	3	50–65% SA–SR gravel
GP loose						
	0–35	*	0	33–36	7	
	"	108–118	0	27.5–32.5	15	
GP medium-dense						
	35–65	*	0	36–39	7	
	"	118–124	0	32.5–37	15	
	50	117–122	288–432	38.7–40.4	3	65–82% A gravel
GP dense to very dense						
	65–100	*	0	39–43	7	
	"	124–134	0	37–42.5	15	
	"	115–125	0	> 37	16	
	*	111–124	0	38–42	6	52–100% SA–SR gravel [alluvium]
	70	126.5	432	40.4	3	65% A gravel
	90	129.1	432	44.4	3	82% A gravel
GM loose						
	0–35	*	0	33–36	7	
	0	114	*	*	11	50% R–SR gravel
	*	51.5–91	104–200	33.6–43	9	Colluvium [graywacke]
GM medium-dense						
	65–100	*	0	36–39	7	
	*	119	430	39.5	13	
GM dense to very dense						
	65–100	*	0	39–43	7	
	"	120–135	0	> 37	16	
GC dense to very dense						
	65–100	115–130	0	> 31	16	
	90% of T99 γ_{max}	123–125	650–720	32.2–34.2	4	50–65% SA-SR gravel
	*	106–118	0–360	33.6–44.7	9	Glacial till [graywacke]

(con.)

Table 5.5—(Con.)

USC	% D_r	γ_d, pcf	C'_s, psf	ϕ', deg.	Source[1]	Material[2]
SW loose						
	0–35	*[3]	0	29–32	7	Fine grained
	"	*	0	31–34	7	Medium gained
	"	*	0	33–36	7	Coarse grained
	"	103–110	0	27–32.5	15	
	*	93.3	320	36.2	13	
	*	95–103	0	33–37	2	Coarse to fine
	0	91.8–103.5	0	32.0–36.2	1	A [crushed]] [Coarse sand with
	0	109	0	27.0–31.0	1	50% A, 50% SR] [20% gravel
	0	112	0	27.1–30.4	1	SR [alluvium]] [4–10% silt
SW medium-dense						
	35–65	*	0	32–35	7	Fine grained
	"	*	0	34–37	7	Medium grained
	"	*	0	36–39	7	Coarse grained
	"	110–116	0	32.5–36	15	
	"	104–108	0	38–41	2	Coarse to fine, peak
	"	"	0	36.5–38	2	Coarse to fine, residual
	50	105–112	130–600	33.0–35.8	3	0-20% SA–SR gravel
	47–63	115–119	0	35.7–38.7	1	SW–SM w/19% A gravel, 12%ML
SW dense to very dense						
	65–100	*	0	35–39	7	Fine grained
	"	*	0	37–41	7	Medium grained
	"	*	0	39–43	7	Coarse grained
	"	116–124	0	36–41	15	
	"	110–130	0	38	16	
	*	110–118	0	39–42	2	Coarse to fine, residual
	*	110–118	0	43–47	2	Coarse to fine, peak
	70	109–119	400–950	35.8–41.4	3	0–49% SA–SR gravel
	79–98	124–130	0	47.5–55.9	1	SW–SM w/19% A gravel, 12% ML
SP loose						
	0–35	*	0	27–30	7	Fine grained
	"	*	0	29–32	7	Medium grained
	"	*	0	31–34	7	Coarse grained
	"	88–110	0	27–32.5	15	
	"	92–98	0	33–35	2	Coarse to medium, residual
	"	92–98	0	33–3 7	2	Coarse to medium, peak
SP medium-dense						
	35–65	*	0	30–33	7	Fine grained
	"	*	0	32–35	7	Medium grained
	"	*	0	34–37	7	Coarse grained
	"	95–116	0	31–36	15	
	"	100–104	0	36–37.4	2	Coarse to medium,residual
	"	100–104	0	37.8–40.3	2	Coarse to medium, peak
	60	107–111	30	37.4	14	SA gravelly SP–SM, 11% ML

(con.)

Table 5.5—(Con.)

USC	% D_r	γ_d, pcf	C'_s, psf	ϕ', deg.	Source[1]	Material[2]
SP dense to very dense						
	65–100	*[3]	0	33–37	7	Fine grained
	"	*	0	35–39	7	Medium grained
	"	*	0	37–41	7	Coarse grained
	"	100–121	0	34–41	15	
	"	100–121	0	37	16	
	"	99–103	0	37.1–39.0	2	Coarse to medium, residual
	"	99–103	0	40.2–43.5	2	Coarse to medium, peak
	*	107–122	0	39–42	6	SA–SR, 0–40% gravel
	*	112–115	0	37.5–39.5	6	R, 0% gravel
SM loose						
	0–35	*	0	27–30	7	Fine grained
	"	*	0	29–32	7	Medium grained
	"	*	0	31–34	7	Coarse grained
	"	88–110	0	27–32.5	15	
	"	88–93	0	32–34.3	2	Medium to fine, residual
	"	88–93	0	32–35.5	2	Medium to fine, peak
	0	79.1–83.9	0	24–26.8	1	A, fine grained
	0	88.5–94.0	0	27.8–29.6	1	A, medium grained
	0	99.5	0	31.6	1	A, coarse grained
	0	92.2	0	28	1	50% A, 50% SR, medium grained
	0	94.6–94.7	0	27	1	SR, medium grained
	0	102.8	0	27.9	1	SR, coarse grained
SM medium-dense						
	35–65	*	0	30–33	7	Fine grained
	"	*	0	32–35	7	Medium grained
	"	*	0	34–37	7	Coarse grained
	"	95–116	0	31–36	15	
	*	93.5–103.5	−130–680	29.9–38.1	13	*
	35–65	94–110	−346–125	27–50	14	Most ϕ's=35–45° SA–SR fine to coarse
	44–57	115–119	0	36.0–40.6	11	R–SR
	35–65	95–98	0	34.9–36.3	2	Medium to fine, residual
	"	95–98	0	36.7–39.0	2	Medium to fine, peak
	*	70–107	0–840	30.6–41.4	8	Undisturbed sandstone colluvium & glacial till
	90% of T99 γ_{max}	63.7–103.6	0–390	34.5–48.9	8	Sandstone colluvium & glacial till
	62–63	99.9–100.3	0	33.6	1	A, fine grained
	54–65	104.3–112.8	0	33.4–34.4	1	A, medium grained
	51–63	112.9–116.7	0	35.4	1	A, coarse grained

(con.)

Table 5.5—(Con.)

USC	% D_r	γ_d, pcf	C'_s, psf	ϕ', deg.	Source[1]	Material[2]
SM dense to very dense						
	65–100	*[3]	0	33–37	7	Fine grained
	"	*	0	35–39	7	Medium grained
	"	*	0	37–41	7	Coarse grained
	"	100–121	0	34–41	15	
	"	110–125	0	34	16	
		98–118	0	32–46	5	
	65–100	99–103	0	37.1–39.0	2	Medium to fine, residual
	"	99–103	0	40.2–43.5	2	Medium to fine, peak
	100% of T99 γ_{max}	70.5–114.8	0–655	30.6–40.5	8	Sandstone colluvium & glacial till
	65–100	90–120	−100–131	30–48	14	55% of ϕ's 38–42°, SA–SR, fine to coarse
	81–98	108–117	0	35.1–49.9	1	A, fine grained
	72–100	115–123	0	37.1–52.4	1	A, medium grained
	67–96	118–128	0	38.1–50.7	1	A, coarse grained
SM						
	*	*	0	34–42	10	Fine to coarse sand
	*	34–106	0–740	24.9–44.4	9	Ash, till, decomposed limestone or colluvial graywacke
SC dense to very dense						
	*	105–125	230	31	16	
	*	103.6	144	32.1	8	Undisturbed glacial till
	90% of T99 γ_{max}	95–97	40–160	23.6–29.2	8	Glacial till
	100% of T99 γ_{max}	107–109	0–185	33.7–39.6	8	Glacial till
	*	68–113	80–360	33.1–40.7	9	Glacial till or decomposed graywacke
ML loose						
	0–35	*	0	26–29	7	
	"	80–86	0	26–30	15	
	*	62.4–68.1	0	31.5–33.7	14	Mt. Mazama ash from Idaho
	0	68.3	0	22.2–25.2	1	Crushed
ML medium-dense						
	35–65	*	0	29–32	7	
	"	86-92	0	30–32.5	15	
ML dense to very dense						
	65–100	*	0	32–36	7	
	"	92–98	0	32.5–36	15	
	"	95–120	190	32	16	

(con.)

Table 5.5—(Con.)

USC	% D_r	γ_d, pcf	C'_s, psf	ϕ', deg.	Source[1]	Material[2]
ML						
	Unknown	55.1–106.4	250–380	30.0–41.1	13	
	"	77–80	55–640	23-43	12	Cohesive clayey silt
	"	59.5–96.9	160–280	32.1–34.4	9	Glacial till–phyllite/schist
	"	86–120	0	33-45	5	
MH–all						
	*	70–90	420	25	16	
	*	68.6	145	34.5	8	Undisturbed glacial till
	90% of T99 γ_{max}	70.5	0	39.6	8	Glacial till
	100% of T99 γ_{max}	77.5	144	36.1	8	Glacial till
	*	48.4-107.3	80–300	34.4–39.2	9	Alluvium
	*	82-115	0	27–47	5	
	82–100	94.5-102.6	0	34.7–43.7	1	A, crushed material

[1] Sources for table 5.5

1 Wu and Baladi 1986; Note: ϕ = angle of repose obtained by measuring the angle of a loosely poured cone of soil; it represents a residual ϕ.

2 Burmister 1962
3 Holtz and Gibbs 1956
4 Holtz and Ellis 1961
5 Holtz and Krizek 1972
6 Leslie 1963
7 equation 5.3 (Prellwitz 1981)
8 Schroeder and Alto 1983
9 Schroeder and Swanston 1987
10 Schultz 1971
11 Siddiqi 1984
12 Singh and Lee 1970
13 USDA FS R1 unpublished data
14 Hammond 1986
15 figure 5.11 (U.S. Department of Navy 1974 and Prellwitz 1981)
16 table 1 (U.S. Department of Navy 1974)

[2] A = angular, SA = subangular, SR = subrounded, R = rounded.

[3] * = values not reported.

used as a first estimate of minimum and maximum values for a uniform PDF when selecting a PDF for ϕ'_p for normally consolidated clays.

5.3.5.3.2 Overconsolidated Clays—The strength of clay, like sand, depends ultimately on the void ratio. But unlike sands, clay readily compresses when the effective confining stress (σ') increases. If σ' subsequently decreases, the clay rebounds, but not back to the original void ratio. Therefore, at a given σ', the overconsolidated clay has a lower void ratio than does the same clay in the normally consolidated state, which results in a greater strength for the over-

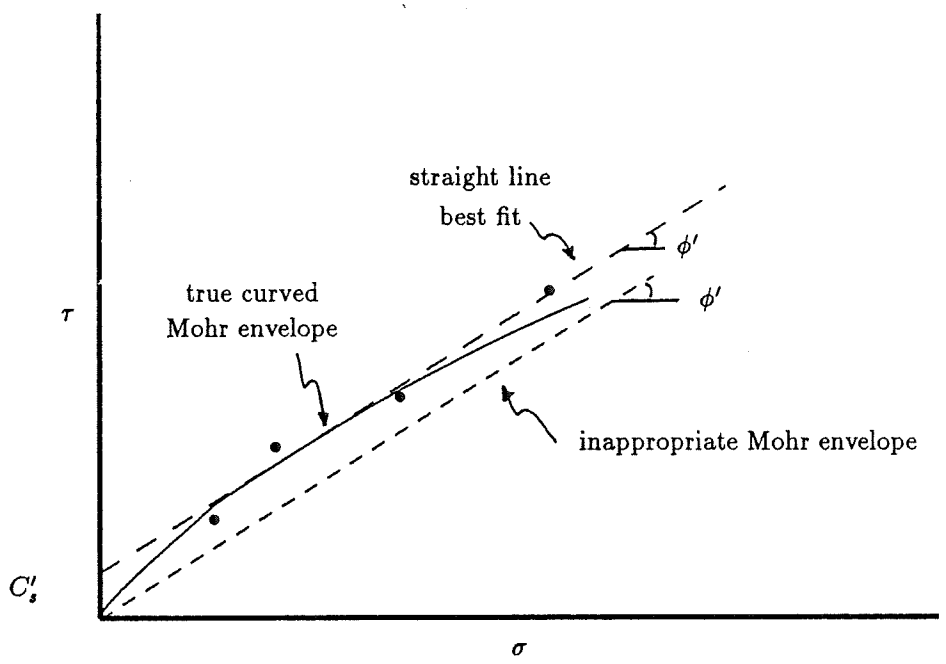

Figure 5.12—Sources of cohesion intercept from laboratory tests on cohesionless soils.

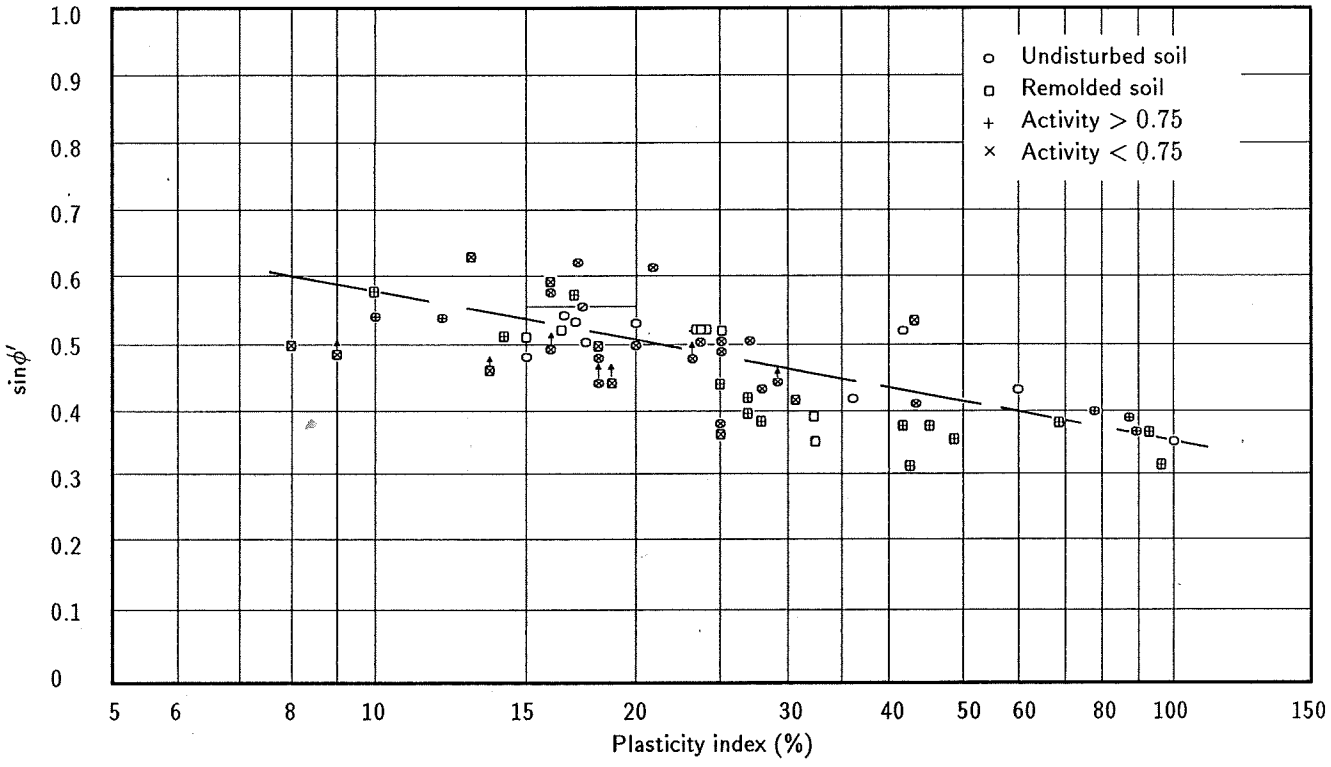

Figure 5.13—Relationship between $\sin\phi'$ and plasticity index for normally consolidated soils (from Kenny 1959).

consolidated clay. This is analogous to a dense sand that has a higher strength than does loose sand at a given σ'.

Geologic conditions that result in overconsolidation include removal of overburden pressure by erosion of overlying material or by melting of a glacier. Other causes include construction loads and fluctuations in the pore-water pressure, which change the effective stress.

Overconsolidation produces *true* cohesion because the clay platelets are pushed together so tightly that molecular forces prevent them from moving apart when the load is removed (Lambe and Whitman 1969; Taylor and Cripps 1987). The magnitude of true cohesion, as well as ϕ', depends on the magnitude of the preconsolidation stress. Reasonable values of true C'_s range from 100 to 500 psf (Lambe and Whitman 1969), although values in the thousands of psf have been reported (Lumb 1966; Taylor and Cripps 1987). These large C'_s values should be used with extreme caution because they frequently result from performing consolidated drained tests so rapidly that pore pressures develop, or as discussed below, are the results of tests at large confining stresses that may not match current *in situ* stress conditions. Reasonable values for ϕ'_p range from 20° to 30° for lightly overconsolidated clay, to 25° to 40° for heavily overconsolidated clay (Taylor and Cripps 1987).

Figure 5.14 compares the Mohr's failure envelope of a normally consolidated clay with that of an overconsolidated clay. The Mohr failure envelope for overconsolidated clay is curved. Typically, the C'_s and ϕ' used are defined by a straight line tangent to the Mohr envelope at the value of stress corresponding to the stress conditions in the field. These C'_s and ϕ' are often called apparent values and typically exhibit a high inverse correlation (Taylor and Cripps 1987) that can be modeled in LISA using the bivariate normal PDF. The apparent C'_s (C'_a) value can be quite large (2,000 to 5,000 psf) when the current stress is close to the preconsolidation stress (low overconsolidation ratio, OCR). In this case, the apparent ϕ' (ϕ'_a) is close to the value for the normally consolidated clay. When the current stress is much less than the preconsolidation stress (high OCR), the C'_a value will be close to the true C'_s, and the ϕ'_a value can be quite large (greater than 40°). In any case, the current stress and the preconsolidation stress, which is determined from a one-dimensional compression test on an undisturbed specimen, must be known to obtain appropriate values of C'_s and ϕ'.

The strength of overconsolidated clays also is affected by weathering and fissuring, typically causing a large reduction in true C'_s and a smaller reduction in ϕ'_p. The weathering process eventually returns the clay to the normally consolidated state with its associated normally consolidated shear strength parameters. Weathering explains the common observation that overconsolidated clays are weaker near the ground surface than at depth.

Because C'_s and ϕ'_p for overconsolidated clays depend on stress history, the current effective stress, and the degree of weathering, it is difficult to obtain typical values from the literature and be assured that they are appropriate for the current *in situ* conditions being analyzed using LISA. Fortunately, there is a simplifying factor. Back-analyses on existing ***first-time*** failures in overconsolidated clays show that the ***average*** shear stress along the entire failure plane is much less than the peak strength of the clay as measured in the laboratory; in fact, the strength parameters corresponding to the average stress often are very close to C'_s and ϕ'_p of the normally consolidated clay (Taylor and Cripps 1987). Therefore, from a practical standpoint, it is probably not necessary to discern whether a clay is overconsolidated and its preconsolidation stress for a Level I

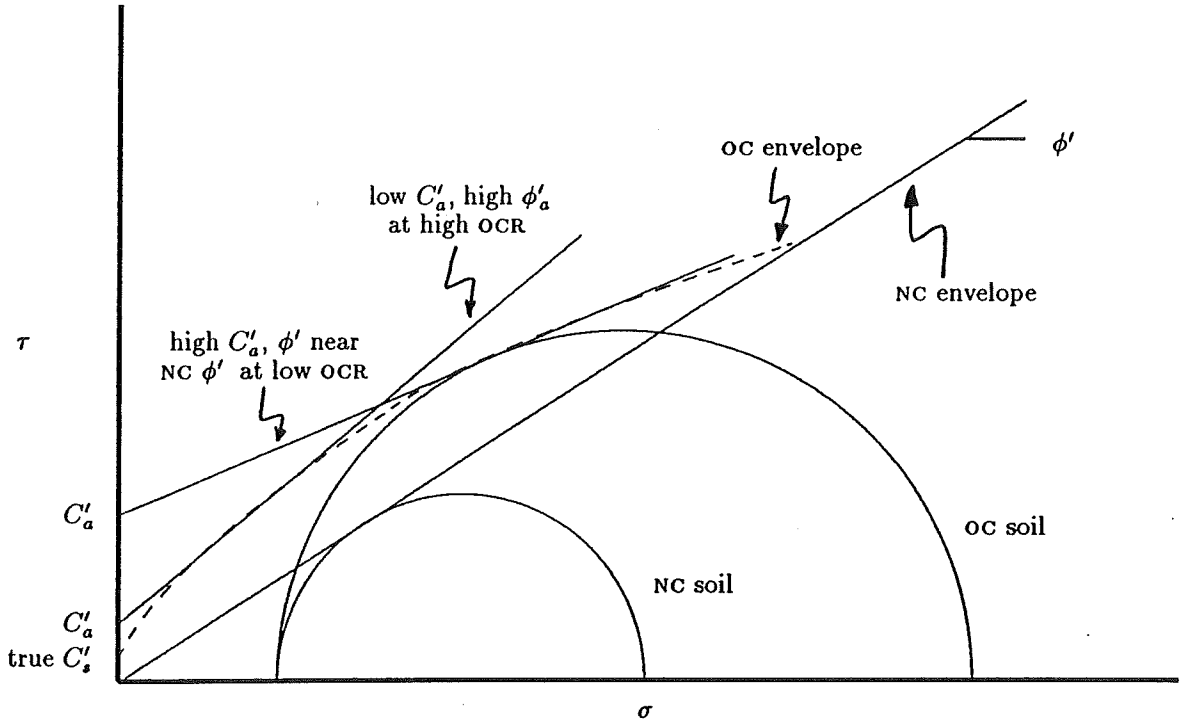

Figure 5.14—Mohr failure envelopes for a clay soil in the normal (NC) and overconsolidated (OC) states.

analysis; rather ϕ'_p can be estimated as for normally consolidated clays using figure 5.13. C'_s may remain between 100 and 500 psf but may be less; C'_s and ϕ'_p should still be considered to be inversely correlated, which can be modeled by using the bivariate normal PDF.

5.3.5.3.3 Unit Weight—The dry unit weights (γ_d) of clay soils typically are reported relative to consistency. Values given in the literature range from 60 to 95 pcf for very soft to soft clay, 30 to 50 pcf for soft organic clay, 75 to 110 pcf for medium clay, and 90 to 130 pcf for stiff to very stiff clay, with values up to 135 pcf for clays containing sand and gravel (Bowles 1968; Dunn and others 1980; Hough 1957; Taylor and Cripps 1987). We suggest using uniform PDF's within these ranges.

5.3.5.4 Residual Shear Strength of Sands and Clays

5.3.5.4.1 Background—The residual friction angle (ϕ'_r; also called ultimate friction angle, ϕ_{ult}) is the friction angle of soil at very large strain and is applicable to sites that have failed previously and those that undergo long-term progressive (occasional or continuous) failure. Figure 5.15 shows idealized stress-strain curves for sand and clay illustrating the change in strength with strain for loose and dense sands (a) and normally and overconsolidated clays (b). The value of ϕ'_r is considered to be a fundamental property of a particular soil in that it is independent of the initial void ratio or confining pressure (Lambe and Whitman 1969; Negussey and others 1988). For clay, ϕ'_r is also independent of the stress history of the clay because, as the clay is sheared, the plate-shaped particles become aligned and the adhesive bonds between clay particles are broken. This results also in C'_s becoming negligible as it is with normally consol-

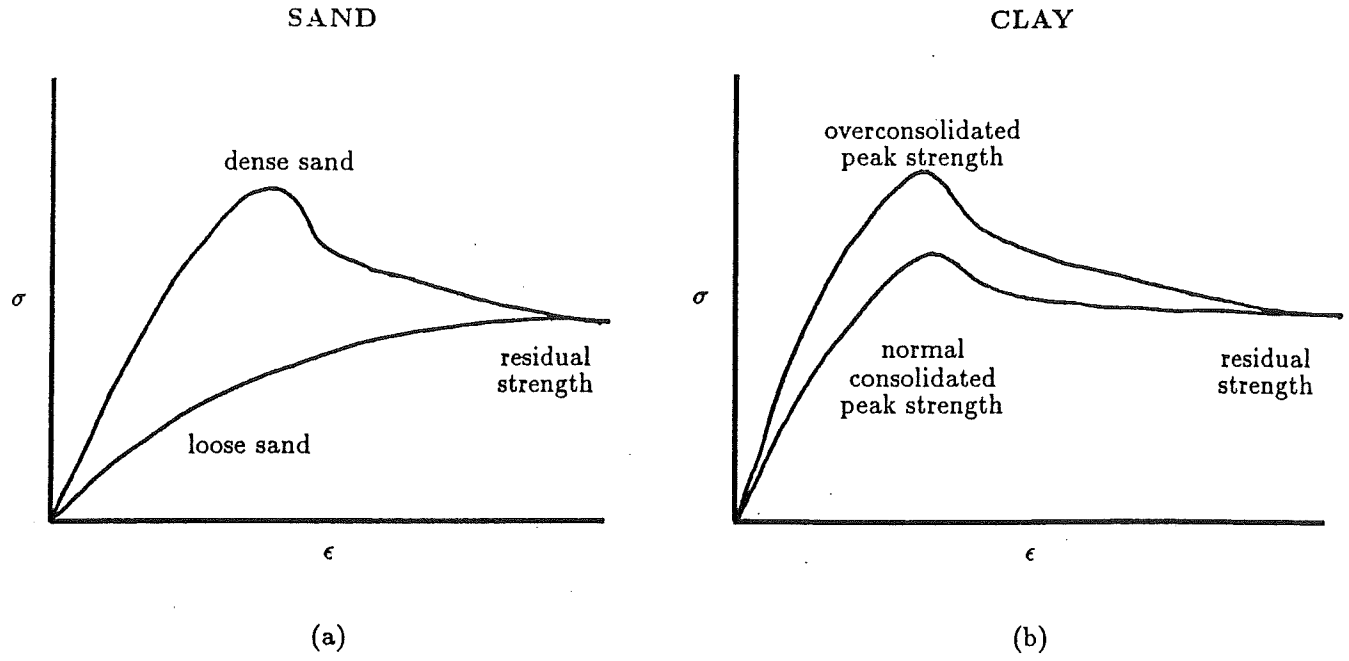

Figure 5.15—Idealized stress-strain curves for sand (a) and clay (b) soils.

idated clays. ϕ'_r is less than ϕ'_p for the same clay whether overconsolidated or normally consolidated. The most reliable laboratory values for ϕ'_r are obtained with a ring shear device, although comparable results have been achieved using triaxial compression tests on initially loose sand specimens (Negussey and others 1988) and by multidirection direct shear tests on clays (Skempton 1985).

5.3.5.4.2 Suggested Values and PDF's—For sands and gravels, values for ϕ'_r can be estimated from equation 5.3, figure 5.11, or table 5.5 at a D_r of 0 percent, and PDF's selected as for ϕ'_p. For soils containing clay, ϕ'_r depends primarily on the clay content and clay mineralogy. Skempton (1985) says that if the clay content is less than about 20 to 25 percent, the clayey soil will behave much like a sand or silt. Therefore, we suggest estimating ranges of values and PDF's for ϕ'_r as one would for silts and sands. When the clay content is greater than 50 percent, ϕ'_r is controlled by the sliding friction of clay minerals and will not change with further increase in clay content. Skempton (1985) and Taylor and Cripps (1987) suggest using 10 to 24° for hydrous mica clays, 14 to 22° with a most likely value of 15° for kaolinites, 9 to 15° with a most likely value of 10° for illite, and 4° (Na) to 10° (Ca) with a most likely value of 5° for montmorillonites (smectites). These ranges can be used to define a uniform or triangular PDF.

When the clay content lies between 25 and 50 percent, ϕ'_r decreases with increasing clay content. Figure 5.16 plots ϕ'_r against clay content from data presented by Skempton (1964, 1985). Collota and others (1989) show a similar relationship between ϕ'_r and clay content but also include liquid limit and plasticity index (fig. 5.17). Either figure could be used to estimate a range of values to define a uniform PDF for ϕ'_r when the clay content is between 25 and 50 percent.

5.3.5.5 Apparent Cohesion

Negative pore-water pressure develops in unsaturated soils due to capillary action (Lambe and Whitman 1969). Negative pore-water pressure (also called

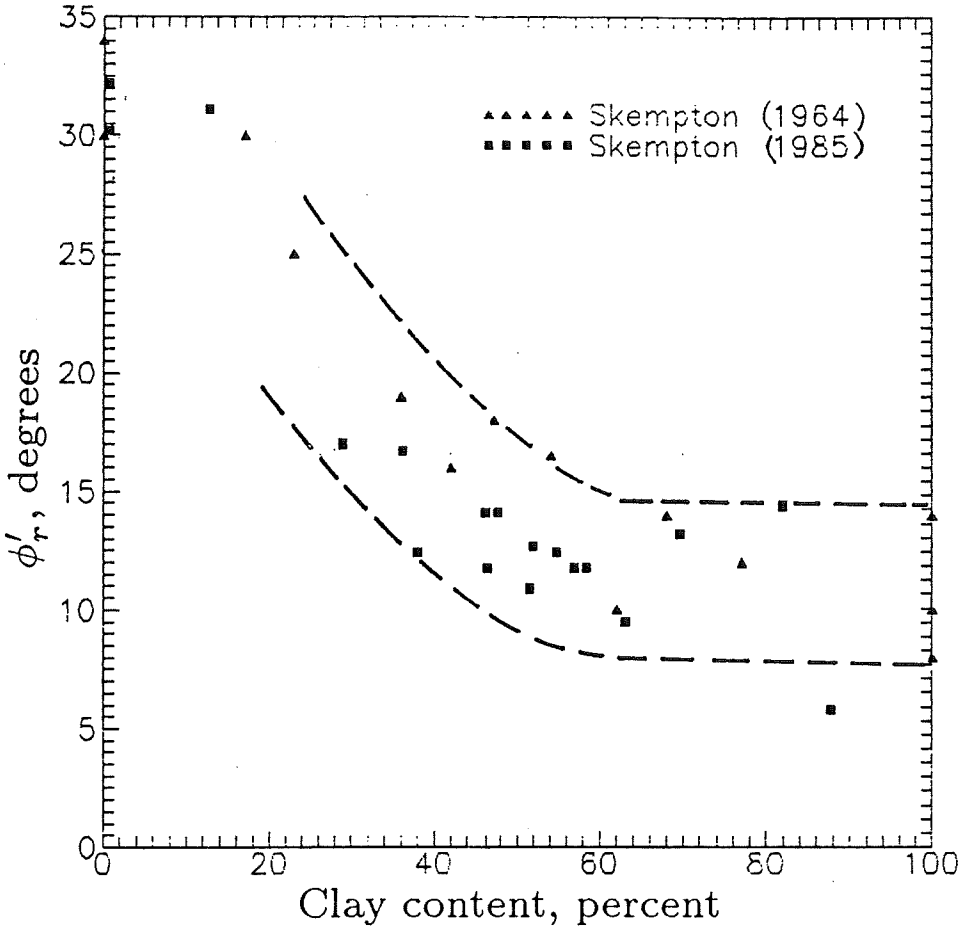

Figure 5.16—Relationship between ϕ'_r and percentage clay (from Skempton 1964, 1985).

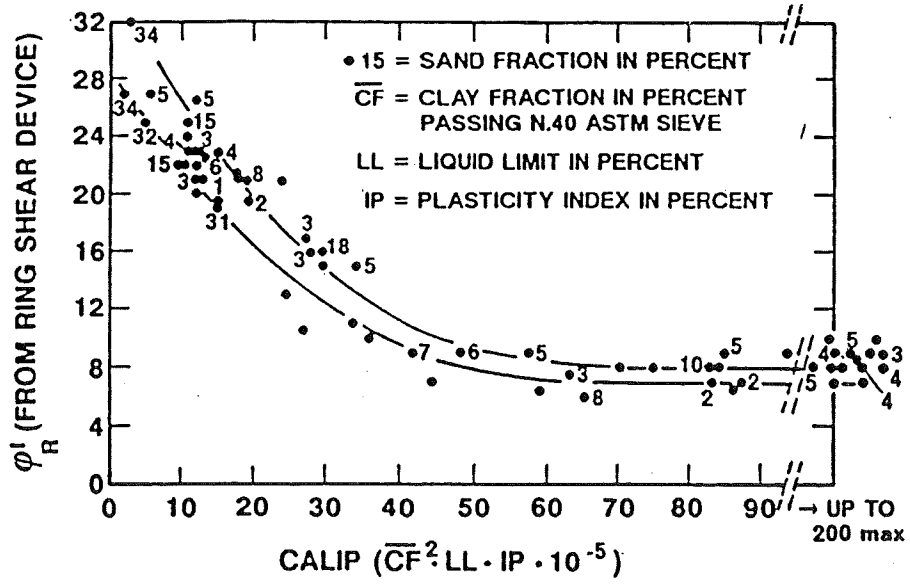

Figure 5.17—Relationship between ϕ'_r, gradation, and index properties of cohesive soils (from Collatta and others 1989).

capillary suction, capillary pressure, or matric suction) produces shear resistance that is called apparent cohesion (C_{app}).

Slope failures have been documented to occur as a result of a decrease in capillary suction, and hence apparent cohesion, without the development of positive pore-water pressure (Matsuo and Ueno 1979). However, this is not the usual case. Slope failures usually occur below the phreatic surface where pore-water pressure is positive and apparent cohesion is zero. Even for the latter case, some C_{app} may be appropriate in the analysis to account for the strength along the portion of the failure surface that passes through the unsaturated zone to the ground surface.

Triaxial compression tests on unsaturated specimens have shown that there is a linear relationship between apparent cohesion and capillary suction (fig. 5.18) (Fredlund 1987). Fredlund terms the slope of this line ϕ^b. Typical values for ϕ^b range from 13 to 23°, with 15° being common. This range of values appears to apply to both sands and clays. By knowing the value of ϕ^b for a given soil and the capillary suction profile in the field, apparent cohesion can be calculated using equation 5.7 or figure 5.19. Values for C_{app} would be added to any true cohesion.

$$C_{app} = (u_a - u_w) \tan \phi^b \tag{5.7}$$

where C_{app} is apparent cohesion due to capillary suction, u_a is pore-air pressure, u_w is pore-water pressure, and $(u_a - u_w)$ is capillary suction. For most practical problems, u_a can be assumed to equal atmospheric pressure (or zero gauge pressure).

The magnitude of hydrostatic capillary suction is equal to the product of the height above the phreatic surface and the unit weight of water, as long as water films on the soil particles are continuous. Thus, the capillary suction at a given point in the soil profile will change as the phreatic surface fluctuates. Also, the capillary suction near the ground surface is usually greater (pore-water pressure more negative) than hydrostatic suction during dry seasons due to dessication, and less (pore-water pressure more positive) than hydrostatic suction during wet seasons due to water infiltration.

Measuring and predicting the soil suction profiles with the seasons and assessing the appropriate profile to use for a particular problem is difficult. Therefore, reasonable values for C_{app} to use in LISA will likely come from back-analysis on existing failures. Cohesion determined by back-analysis would include both true and apparent cohesions.

5.3.5.6 Obtaining Values for Correlation Coefficient (r)

As discussed in section 4.2, values of -0.2 to -0.85 have been reported for the r between C'_s and ϕ' (Cherubini and others 1983). If the user wishes to model the correlation, but no laboratory data exist, we suggest that values in this range be used with the bivariate normal PDF to perform a sensitivity analysis to evaluate the effect of the correlation on the probability of failure. We advise using the same random seed number for each run to eliminate the variation in probability of failure that usually occurs with repeated simulations.

If laboratory data exist, it is simple to obtain values for the correlation coefficient between C'_s and ϕ'. First, plot C'_s against ϕ' to observe whether a linear correlation exists and the degree of scatter in the correlation. Then perform a linear regression on the $C'_s - \phi'$ data. Graphics programs and spreadsheets such as Golden Software's GRAPHER and LOTUS 1-2-3, respectively, perform regressions and report the coefficient of determination (r^2). Programmable calculators, such as the HP41 with STAT PAC, also can be used. The correlation

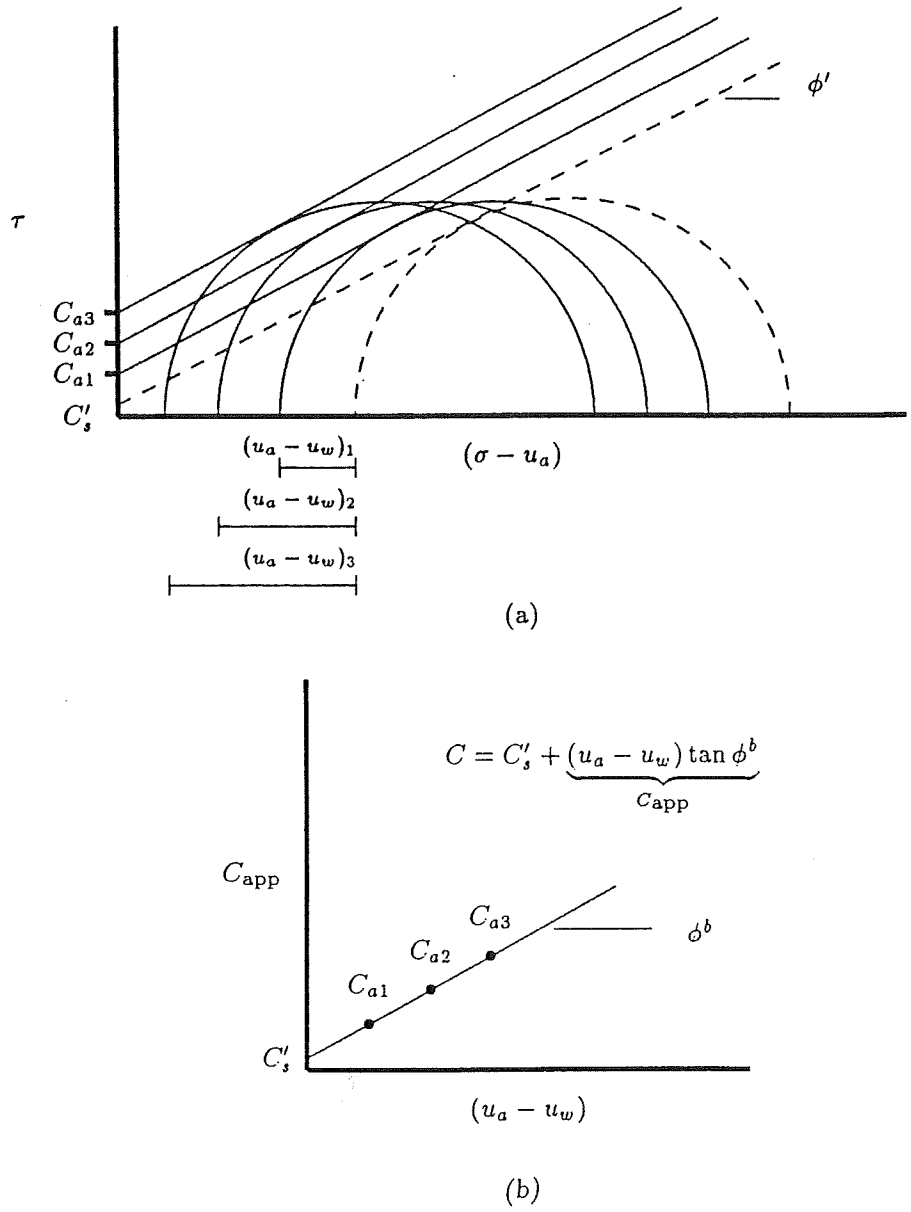

Figure 5.18—Mohr's failure circles on unsaturated soils showing apparent cohesion (a). Determination of ϕ^b (b).

coefficient, r, is simply the square root of r^2 and has the sign of the slope of the regression equation.

Apparent soil cohesion due to capillary suction is not inversely correlated to ϕ', so r may be taken as zero and univariate distributions used for C'_s and ϕ' in LISA simulations.

5.3.6 Moisture Content

Moisture content is used to compute the moist soil unit weight (γ or γ_m) of the soil above the phreatic surface. The moisture content is not uniform throughout the soil but varies with depth depending on the soil gradation and climate and groundwater conditions. For instance, fine-textured soils can maintain a significant thickness of saturated soil above the phreatic surface, the "capil-

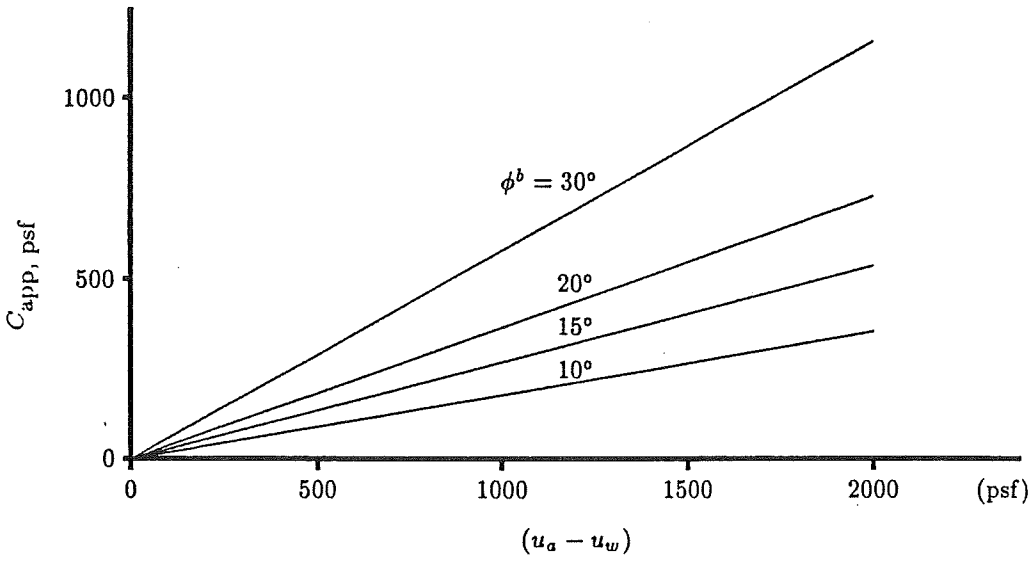

Figure 5.19—Relationship between capillary suction and apparent cohesion for various values of ϕ^b.

lary fringe," which is due to capillary suction; whereas coarse-textured soils can maintain little or no capillary fringe. However, since the infinite slope equation is relatively insensitive to the value of moist unit weight used in the analysis, the assumption of a uniform moisture content within the soil profile should cause no significant inaccuracies.

Reasonable values for moisture content can be obtained by calculating the saturated moisture content of the soil over the range of unit weights to be used; the DLISA program does this for you automatically. Then select a range of values some percentage less than the saturated moisture content values. For instance, if you are assuming a major rainfall or snowmelt event for the analysis, it would be reasonable to select moisture contents just a few percent less than the saturated moisture content.

Because dry unit weight and moisture content are simulated independently, it is possible to simulate on any given pass a value for moisture content that is greater than the saturated moisture content. If this happens, LISA will use the saturated moisture content to compute the moist unit weight of the soil. It should be obvious that this has happened if, when you view the histogram or scatter plot of the moist and saturated unit weights, some (or many) of the values for moist unit weight are the same as for the saturated unit weight.

5.3.7 Groundwater

Positive pore-water pressure due to increasing groundwater levels is widely recognized as the triggering mechanism for most slope failures based both on direct measurements of initiation or acceleration of slope movement coincident with increasing pore-water pressure (Iverson and Major 1987; Reid and others 1988), and on the observation that slope failure occurrences increase during periods of intense rainfall or major rain-on-snow events (Brand and others 1984; Campbell 1975; DeGraff and others 1984; Ellen and Wieczorek 1988; Keefer and others 1987; Pierson 1980; Sidle 1984a, 1986; Ziemer 1984).

The groundwater environment modeled with LISA is assumed to result from rain or snowmelt infiltration rather than a permanent groundwater system. The

subsurface flow (often called "through flow") is ephemeral, resulting from water infiltrating the surface soil, perching on a water-impeding layer, and flowing laterally toward streams or depressions.

The groundwater distribution used in LISA *represents the spatial variation of the peak groundwater–soil depth ratios (D_w/D) expected across the landform during some infiltration event, either by rainfall or snowmelt.* To illustrate this statement, consider a landform in which 80 percent of the slopes are straight or convex and do not concentrate groundwater, while in 20 percent of the landform groundwater flowlines converge in a draw, resulting in high groundwater levels. During a major infiltration event, the soils in these concentration areas are expected to become saturated to or near the ground surface. This landform might be represented by a frequency histogram with two classes: one class with D_w/D ratios between, say 0.1 and 0.3, with an 80 percent frequency; the second class with D_w/D ratios between 0.7 and 1.0 with a 20 percent frequency. Conceptually, the groundwater distributions would be different for different landforms depending on whether the flowlines tend to converge or diverge. The groundwater distribution also would vary depending on whether an average or major infiltration event was considered.[7]

Obtaining the input data needed to estimate the probability distribution for D_w/D can be time-consuming and difficult. Drill holes equipped with standpipe piezometers or slotted pipe observation wells provide a fairly reliable means for obtaining field data on water levels. However, these data are seldom available at the reconnaissance mode of Level I. The user will have to depend heavily on experience and limited qualitative information that can be obtained by ground inspections of the polygon. The presence of springs, seeps, boggy areas, and thriving vegetation indicate groundwater levels at the ground surface. Seasonal fluctuations in this seepage activity may provide some clues to the groundwater system. Soil pits also can provide clues about the maximum level to which groundwater usually rises at a site. A gray soil color, typical of a reducing environment, can indicate nearly continuous saturation. Orange and yellow mottles typical of an oxidizing environment can indicate seasonal or periodic saturation of the soil, although soils can experience periodic saturation without mottles developing.

Trial computations with LISA can be directed toward a sensitivity study of the water level's effect on slope stability in the polygon. These results, combined with field information and the user's experience and judgment, should yield a reasonable range of water level values and perhaps a most likely value, leading to a triangular probability distribution.

Back-analysis of groundwater heights at existing failures can indicate a range of groundwater heights to expect in the regions of a landform where groundwater concentrates. Failed sites are useful because at the time of failure, the factor of safety must have equaled 1.0. The soil and site conditions at the time of failure need to be estimated and used in the back-analysis. Using DLISA, the ranges of D_w or D_w/D needed to give a factor of safety of 1 can be determined quickly for a variety of combinations of other input variables. The portion of the landform over which this range of D_w/D might be found can be estimated from the topography, seeps, vegetation, and other conditions described earlier.

Although field observations of groundwater conditions are preferable, the user may begin a LISA assessment using a catalog of groundwater distributions for

[7] A method for conditioning the LISA probability of failure estimates with the probability of certain infiltration events occurring during some specified length of time is discussed in appendix D.

the landforms on their forests. The user may develop such a catalog by relating a distribution to a particular landform shape, considering also aspect, elevation, position on the slope, vegetation, and other influencing factors. For example, a concave slope with numerous draws that converge groundwater flow lines (causing areas of high groundwater levels) should have a distribution that gives a higher probability of high groundwater than would a straight slope or a convex slope where groundwater flow lines diverge. Wooten (1988) took this approach on the Gifford Pinchot National Forest and found it useful for preliminary assessment. Figure 5.20 illustrates hypothetical groundwater–soil depth distributions for two landforms. The groundwater distributions shown are *not* based on any groundwater monitoring or modeling.

When attempting to formulate probability distributions for D_w/D, the user should remember that this ratio is somewhat controlled by soil thickness. In particular, all other factors being equal, landforms with thin soils should have higher D_w/D ratios than do those with deep soils. Also, care should be taken not to overestimate the portion of land area with high D_w/D. A recent study by Petch (1988) concerning the spatial distribution of soil saturation suggests that for small, steep (30° slope) first-order basins, the portion of the land area in which the soils are saturated to or near the surface ($D_w/D > 0.8$ or 0.9) with a large storm or snowmelt event may be on the order of 5 percent. The portion of the land area with little or no saturated soil ($D_w/D < 0.1$ or 0.2) may be on the order of 40 percent. Gentle basins ($< 10°$) or basins containing areas of poorly drained soils may have larger portions (25 to 75 percent) of nearly saturated conditions (Dunne, in Kirkby 1978; Hookey 1987; Peck and Williamson 1987).

Studies also have shown that in some cases, soil saturation patterns are less dependent on topographic convergence than on the spatial variation of soil hydraulic conductivity or soil water storage (Petch 1988; Reid and others 1988). Therefore, individual sites may not follow gross generalizations made between landform and spatial distribution of D_w/D. Large-scale groundwater flow systems, such as groundwater base flow from bedrock fractures (Hodge and Freeze 1977; Okunushi and Okimura 1987) and flow in soil pipes (Jones 1988; Pierson 1983), also may be important at some sites.

5.3.7.1 Effects of Timber Harvest on Groundwater Levels

Clearcutting has the potential for increasing the areal extent and the thickness of the saturated zone by increasing the amount of water available for infiltration. The increase in available water results from a decrease in rain or snow interception and evaporation, increases in snow accumulation and the rate of snowmelt, and to a lesser extent, a decrease in transpiration (Megahan 1983). The increase in available water and the resulting increase in streamflow due to clearcutting have been well documented. (Some recent references include Berris and Harr 1987; Harr 1986; Toews and Gluns 1986; Troendle 1987; Troendle and King 1987.)

Several studies have shown increases in groundwater rise and the extent of saturated soil conditions due to clearcutting. Some of the studies looked at gentle watersheds with thick soils and found increases in the minimum water table measured during the summer months (Borg and others 1988; Holstener-Jorgensen 1967; Peck and Williamson 1987). Borg and his coworkers measured an increase in minimum groundwater levels for 2 to 4 years and then declining levels as the forest regenerated. They estimated that groundwater levels will

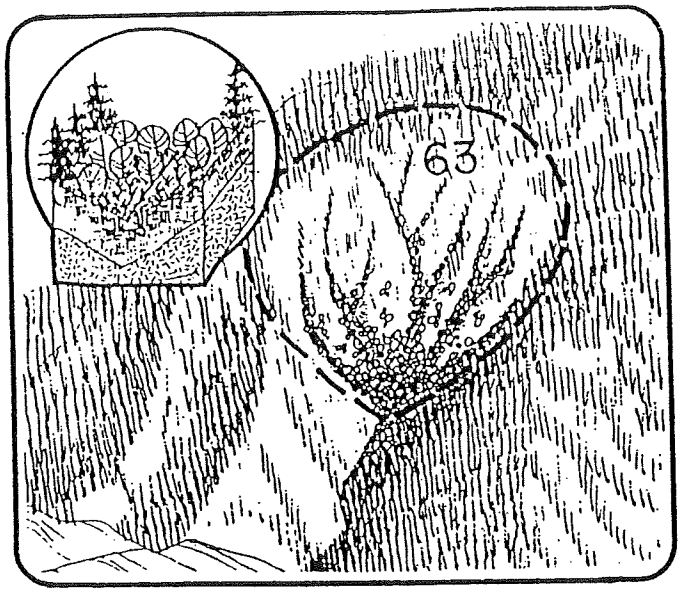

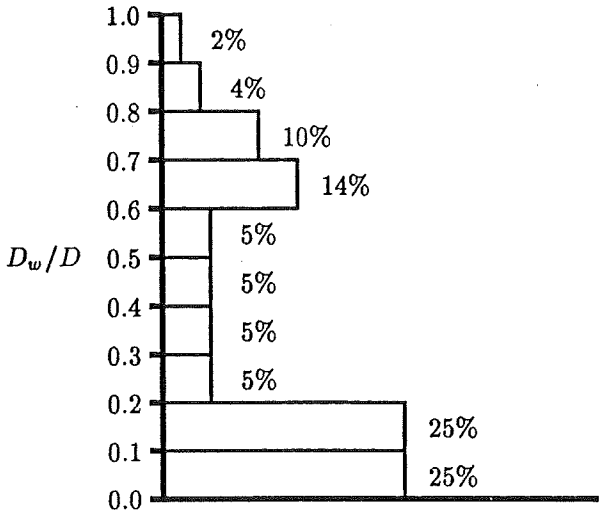

LANDFORM 63 STREAM HEADLANDS

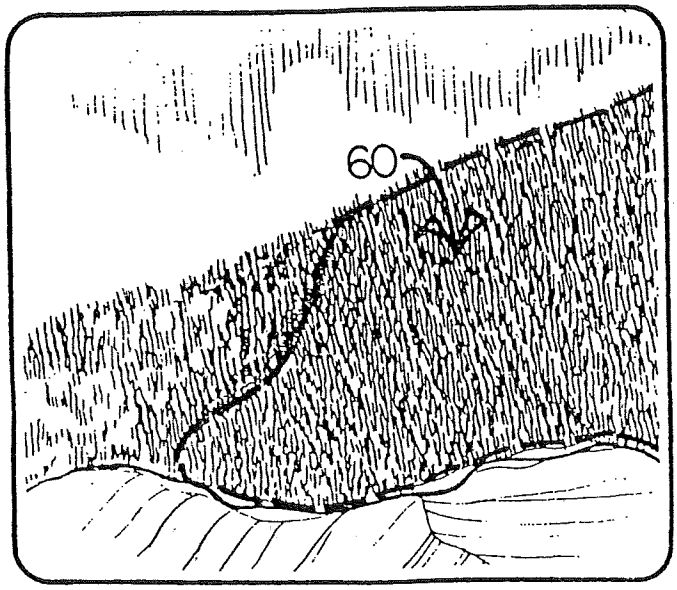

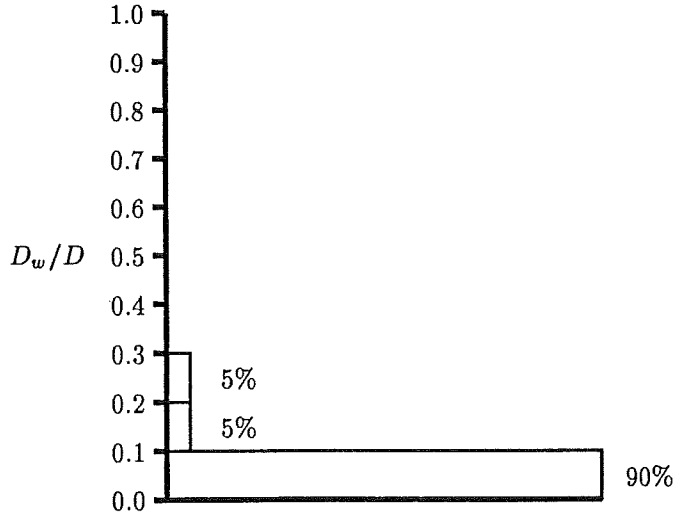

LANDFORM 60 NONDISSECTED STREAM BREAKLANDS

Figure 5.20—Illustrations of landforms and corresponding hypothetical groundwater distributions. The landforms are from the Clearwater National Forest in the Northern Region of the Forest Service (Wilson and others 1983).

reach the levels they would have been without logging within 15 years after the beginning of regeneration.

Peck and Williamson (1987) measured increases in both the annual minimum and annual peak water tables in a basin converted from forest to agriculture. The water levels increased steadily over the 10 years following timber harvest, suggesting that water accumulates until a new input-output equilibrium is achieved.

Other studies have monitored the effect of clearcutting on shallow, perched subsurface runoff that typically results in short-term saturated conditions. These studies also seem to show an increase in the peak groundwater levels recorded during rainfall or snowmelt events (Gray and Megahan 1981; Megahan 1984; Wu 1984). Troendle (1987) reported increases in intercepted subsurface lateral flow due to clearcutting. Groundwater levels were measured but not reported; however, it is logical to assume that if groundwater flow volume increased, groundwater levels would also. Petch (1988) compared the groundwater response to rainfall of a forested basin and a grass basin and found the weekly peak water table levels were usually lower in the forested basin. He attributed the difference primarily to the high interception loss of 49 percent in the forest. Mathematical models also demonstrate the link between timber harvest and increases in soil moisture and groundwater level (Hillman and Verschuren 1988).

The magnitude of the groundwater rise resulting from clearcutting is difficult to predict because, first, it is site specific, depending on the soils, geology, and topography of the site. Second, groundwater levels will vary with annual variations in rain or snowfall, snowmelt, and evapotranspiration. Therefore, it becomes difficult with a limited amount of preharvest and postharvest monitoring data to separate the effects of clearcutting from climatic variations. However, Megahan (1984) did estimate an average increase of 68 percent in the annual peak piezometric levels resulting from clearcutting for 3 postharvest years.

With so little monitoring data available, it is difficult to recommend how much to increase a groundwater distribution to assess with LISA the effects of clearcutting. That is, it appears that groundwater levels at specific points in the basin increase on the order of 50 percent, but the portion of the basin showing higher groundwater levels is a function of site characteristics. Narrow draws with steep side-slopes might show an increase in groundwater level but little increase in the area with high groundwater. Broad, gentle basins might show less increase, but the increase may affect a greater portion of the basin (Dunne in Kirkby 1978; Peck and Williamson 1987).

It is only through additional groundwater monitoring supplemented by modeling that we may begin to gain knowledge on the spatial variation of groundwater levels. Additional research is needed to improve tools to quantify spatial variability and the likelihood of occurrence of peak groundwater levels expected during a specified period, with and without timber harvest.

CHAPTER 6 — EXAMPLE APPLICATION: DARK 3 PLANNING AREA, GIFFORD PINCHOT NATIONAL FOREST

6.1 Introduction

The Dark 3 planning area is on the Randle Ranger District, Gifford Pinchot National Forest, in Washington (Pacific Northwest Region). Jones (1990) performed a Level I stability analysis over the entire area and evaluated three timber sale alternatives. Figure 6.1 shows the topographic map of the Dark 3 planning area and the Level I polygons. (Unlabeled polygons are primarily flood plain deposits and were not analyzed.) The District then requested additional analysis (Level II) on one harvest unit for which field observations supported by the initial LISA analysis indicated a high probability of failure after timber harvest. The District desired to harvest the potentially unstable unit for silvicultural reasons. Both analyses will be described in this chapter. (Using LISA to perform a Level II analysis is discussed in section 5.1.3.)

6.2 Geology, Soils, and Topography

The bedrock geology and soil conditions of the Dark 3 planning area are shown in the Geologic Resources and Conditions (GRC) map (fig. 6.2). The bedrock geology of the western half of the area consists of extrusive igneous and minor pyroclastic rocks dipping to the west at 5 to 15 degrees. This bedrock forms a tablelike topographic surface with surface slopes ranging primarily from 20 to 50 percent. The overlying soils consist of 2 to 5 (locally 10+) feet of colluvium and residuum (GW–SM) with minor amounts of glacial till (SM–GM and GMu). It was anticipated that this region would have few stability problems because of the gentle slopes and therefore was analyzed with only two LISA polygons (designated as 3M and 4W in fig. 6.1).

A crescent-shaped area of steep ground with slopes generally greater than 70 percent extends from the northwestern to the southeastern boundary of the planning area. The soils of this steep crescent, which is the edge of the table of volcanic rocks, generally consist of 1 to 2 feet of coarse tephra overlying 2 to 3 feet of colluvium and minor residuum developed from the underlying volcanics (SM–GW). While most of the area appears dry and well drained, areas of springs and seeps are observed. The elevated groundwater and steep slopes apparently have caused rockfalls and debris avalanches, several of which are mapped on the GRC map. Because of the steep slopes and past failure activity, there was concern that timber harvest or road construction in the area would increase the mass failure potential with the possible impacts of loss of the soil resource and damage to the water quality and fisheries of Summit Prairie Creek. Therefore, the crescent was divided into several small polygons of four types (1D, 1M, 2D, 2M), differentiated by slope and groundwater conditions.

In the northeastern third of the area, the bedrock consists of pyroclastic rocks with minor intrusive and extrusive igneous rocks. The bedrock is overlain by glacial till, colluvium, and residuum with minor alluvium, averaging 5 to 10 (locally 30+) feet in thickness. The topography consists of moderate slopes (40 to 90 percent). The area is generally considered to be dry with low failure potential and therefore was analyzed with one LISA polygon (5D).

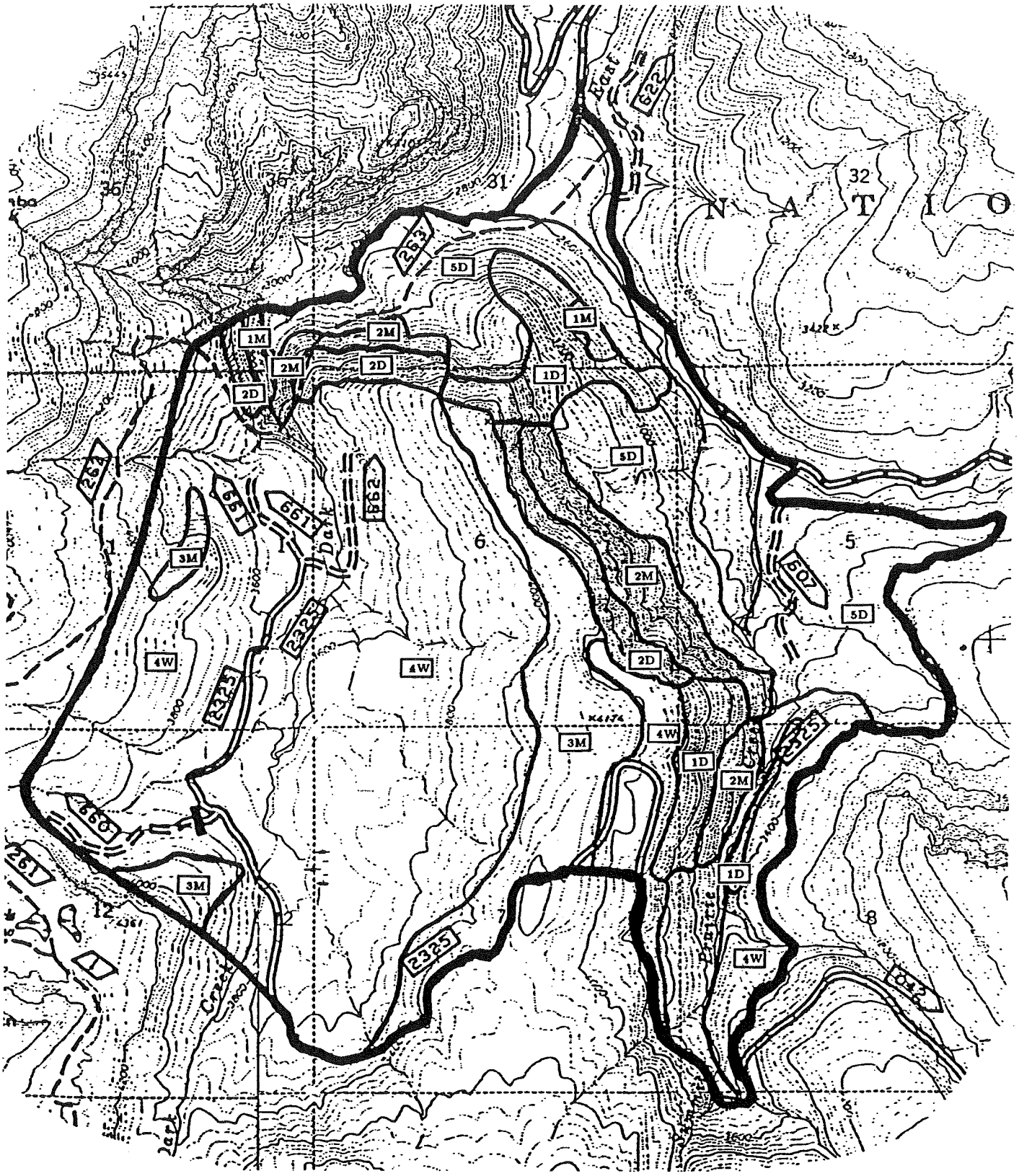

Figure 6.1—Dark 3 planning area and Level I polygons.

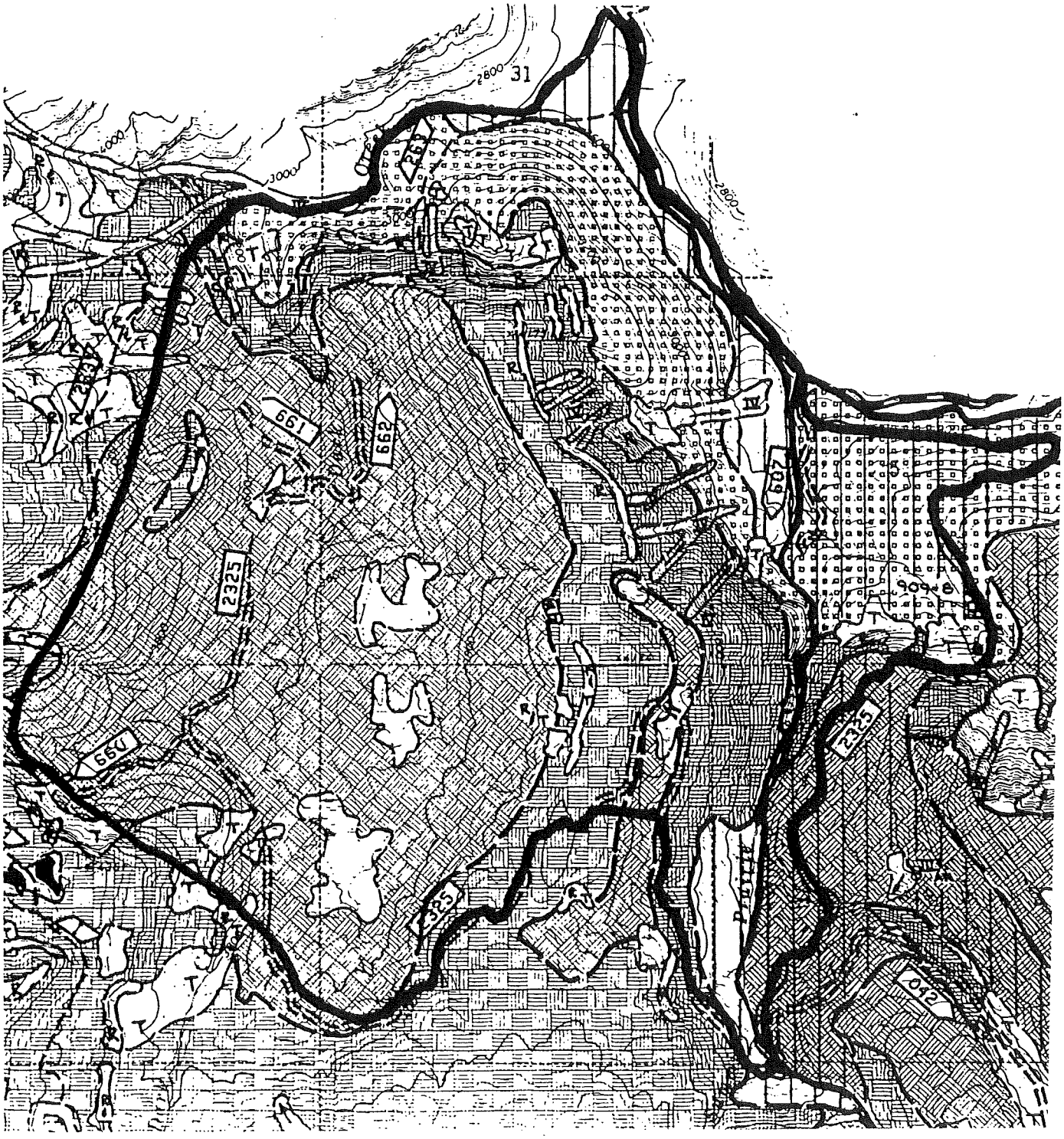

Figure 6.2—Geologic Resources and Conditions (GRC) map for the Dark 3 planning area.

Mapping Boundary

——— Ground Verified

– – – – Inferred

Geologic Resources

Mineral Materials

□ — Developed Source

○ — Undeveloped Source

⊠ — Depleted Source

⊞ — Closed Source

△ — Terminated Source

Geologic Point of Interest

Underground Space

Groundwater Extraction

Geologic Conditions

R — Exposed Rock

T — Exposed Talus

Wet Area

Spring

Slope Stability

I ——— Slide
II ——— Flow
III ——— Rockfall
IV ——— Avalanche
V ——— Sidecast Failure > 55% Slope
VI ——— Fill Failure < 55% Slope
VII ——— Cutslope Failure

A = Active Slide
PA = Past Active Slide
N = Naturally Occurring
M = Man Related

NAME/ORIGIN: Colluvium and residuum overlying extrusive igneous and minor pyroclastic rock.

SOIL: Nonplastic loose silty sand to well graded gravel (USC:SM–GW). Avg depth < 5′.

ROCK: Basalt (URC:BBEA); andesite (URC:BBEA–DDEC); basalt breccia, tuff, tuff breccia (URC:BCEB–CCEB), BRU 2021.

SIGNIFICANT CONDITIONS: Unit is characterized by sparsely vegetated steep slopes with thin rocky soil, numerous avalanche chutes, rock outcrop and talus slopes. Wet talus slopes are common. Unit is similar to map unit  except that this unit has steeper slopes and thinner soil. Minimum surfacing will probably be required for subgrade strength. There is a good potential for quality material sources, but development may be difficult due to steep slopes.

Special Considerations

- The compartment is overlain with 2–4′ of past and recent Mount St. Helens pumice and ash consisting of poorly graded sand to silty sand (USC:SP–SM). Tephra is free-draining, easily eroded, and may be washed and accumulated into thicknesses up to 12′+.
- Several sidecast failures occur along the 29 Rd. adjacent to McCoy Creek.

Figure 6.2—(Con.)

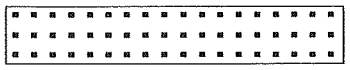

NAME/ORIGIN: Colluvium, residuum, and local deposits of glacial till overlying pyroclastic and minor intrusive and extrusive igneous rock.

SOIL: Colluvium and residuum—nonplastic to slightly plastic silty sand to silty gravel (USC:SM/SM_u–GM/GM_u). Avg depth: 3–9′, locally 12′+. Glacial till—nonplastic silty sand to silty gravel (USC:SM–GM), and slightly plastic silty gravel (USC:GM_u), local nonplastic silt (USC:ML). Avg depth: 3–8′, locally up to 30′.

ROCK: Tuff, tuff breccia, subordinate felsic tuff (URC:BCEA–DDED); basalt, andesite (URC:BBEA), BRU 4005D.

SIGNIFICANT CONDITIONS: Plastic soil is not free-draining, susceptible to slope failure when disturbed on steep slopes, and generally a weak subgrade material. There is a low potential for material sources in this unit. Refer to map unit for significant conditions for glacial till.

NAME/ORIGIN: Glacial till, colluvium, residuum, and minor alluvium overlying pyroclastic and minor intrusive and extrusive igneous rock.

SOIL: Glacial till—nonplastic silty sand to silty gravel (USC:SM–GM), and slightly plastic silty gravel (USC:GM_u), local nonplastic silt (USC:ML). Avg depth: 5–10′, locally 30′+. Colluvium and residuum—nonplastic to slightly plastic silty sand to silty gravel (USC:SM/SM_u–GM/GM_u). Avg depth: 4–8′. Alluvium—poorly graded sand to poorly graded gravel (USC:SP–GP). Avg depth: < 5′.

ROCK: Tuff, tuff breccia, local felsic tuff (URC:BCEA–DDED); basalt, andesite (URC:BBEA), BRU 4005D.

SIGNIFICANT CONDITIONS: Till is locally plastic and/or compact and not free-draining resulting in elevated water tables. Loose till is subject to ravelling resulting in increased road maintenance. Plastic soil is susceptible to slope failure when disturbed on steep slopes, and is generally a weak subgrade material.

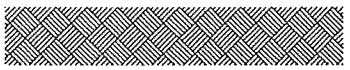

NAME/ORIGIN: Colluvium, residuum, and local deposits of glacial till overlying extrusive igneous and minor pyroclastic rock.

SOIL: Colluvium—silty sand to silty gravel (USC:SM–GM). Avg depth: 3–5′, locally up to 15′. Residuum—nonplastic to slightly plastic silty sand (USC:SM/SM_u). Avg depth: 2–4′, locally up to 12′+. Glacial till—nonplastic silty sand to silty gravel (USC:SM–GM), and slightly plastic silty gravel (USC:GM_u). Avg depth: 2–5′, locally up to 10′+.

ROCK: Basalt (URC:BBEA); andesite (URC:BBEA–DDEC); basalt breccia, tuff, tuff breccia (URC:BCEA–DDED), BRU 2021.

SIGNIFICANT CONDITIONS: Unit is characterized by gentle to moderate slopes with poor surficial drainage indicated by the presence of wet areas. Plastic residuum is not free-draining and is generally a weak subgrade material. Glacial till—refer to significant conditions of map unit . Till occurs mainly in the Dark Creek drainages.

6.3 Polygon Delineation and Distribution Selection—Level I

Jones (1990) delineated polygons for the initial Level I analysis using 1:7,200 topographic maps and the soil/geology type as mapped in the GRC. In areas with slopes greater than 65 percent, additional polygons were delineated using low-altitude aerial photographs to better describe slope and groundwater characteristics. Initial soil type and soil depth estimates were obtained from the GRC map and the Soil Resource Inventory (SRI). Shear strength and unit weight values and distributions then were estimated from the USC classification and previous experience and by using table 5.4 and figure 5.11 of this manual. Groundwater distributions used were developed from the groundwater characteristics mapped on the GRC, field observations, and by using a catalog of distributions tied to various landforms developed by Wooten (1988). Root strength distributions used were those suggested by Wooten (1988) for a type B soil–root morphology class. Figure 6.3 contains Wooten's suggested distributions. Limited field checking was performed to verify office findings. Table 6.1 gives the distributions used in the analysis.

6.4 Level I Results

Table 6.2 lists the ranges of the probabilities of failure for each polygon as estimated using the LISA program for both the natural and clearcut states. The range of probability of failure values was obtained from five simulations, each using a different seed number for the random number generator. The probabilities of failure for clearcut harvest are conditional on a "major" rainfall or rain-on-snow event occurring during the period of minimum root strength. Also given are relative probabilities of landslide hazard based on the experience and interpretation of the Gifford Pinchot National Forest geotechnical group. This scale can aid individuals not familiar with the LISA program and those uncomfortable with probability numbers in interpreting LISA results. It is not an absolute scale that would necessarily be applicable elsewhere; it is only a *relative* scale based on the experience of the geotechnical group on the Gifford Pinchot.

The proposed cutting units for three timber sale alternatives were overlain on the LISA polygons, and the land area in low, moderate, and high failure-potential polygons was measured. These results are summarized in table 6.3. For each proposed cutting unit, the potential impacts should a failure occur were evaluated as either localized or as having the potential to deliver sediment to Summit Prairie Creek. One of the harvest units (unit 7) of timber sale alternative 1 was located partially in the high failure-potential polygon 2M, with the potential impact of delivering sediment to the creek. Because of this LISA result, along with observations of instability along road 2325 above unit 7, further analysis of the unit was deemed necessary. This analysis is discussed in the next two sections.

6.5 Polygon Delineation and Distribution Selection—Level II

Jones (1990) spent approximately 3.5 days in the field gathering slope, soil type, soil depth, and groundwater information to further evaluate the portion of the Dark 3 planning unit surrounding harvest unit 7. Based on the field evaluation, Jones modified the polygons in that portion as shown in figure 6.4. Slopes were measured with a clinometer and soil depth with a hand auger at random

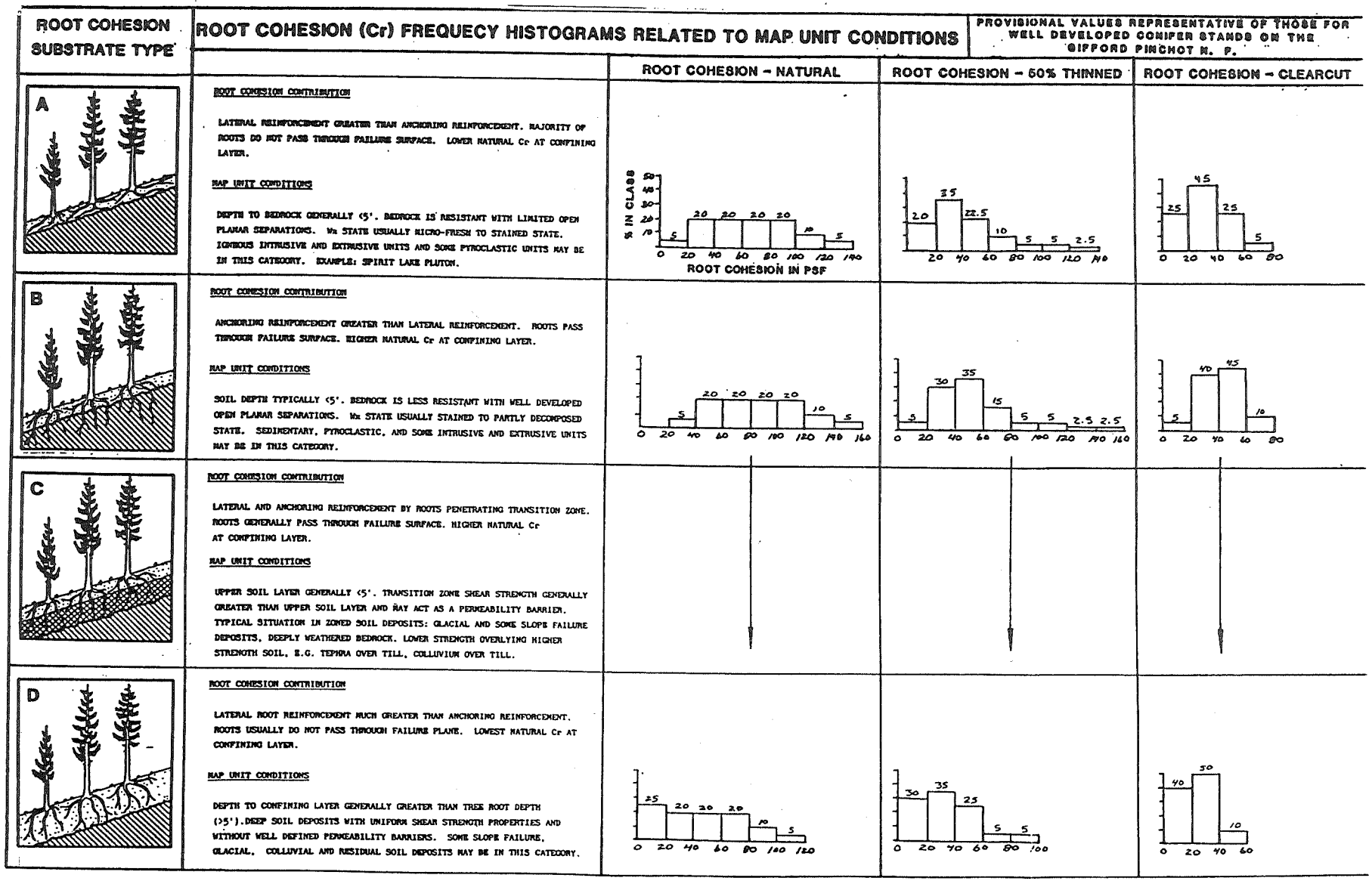

Figure 6.3—Root cohesion distributions suggested by Wooten (1988) for use on the Gifford Pinchot National Forest.

Table 6.1—Distributions used in the Dark 3 Level I analysis

Polygon	D	α	C'_s	ϕ'	D_w/D	
					Natural	Clearcut
1D	$T[1,3,5]$	$T[65,75,95]$	$U[10,75]$	$U[31,38]$	$T[0,.2,.4]$	$T[0,.25,.5]$
1M	$T[1,3,5]$	$T[65,75,95]$	$U[10,75]$	$U[31,38]$	$T[0,.2,.5]$	$T[0,.3,.6]$
2D	$T[1,3,5]$	$T[70,85,110]$	$U[10,75]$	$U[31,38]$	$T[0,.2,.4]$	$T[0,.25,.5]$
2M	$T[1,3,5]$	$T[70,85,110]$	$U[10,75]$	$U[31,38]$	$T[0,.2,.5]$	$T[0,.3,.6]$
3M	$T[2,4,10]$	$T[20,30,70]$	$U[10,50]$	$U[34,42]$	$T[0,.2,.5]$	$T[0,.3,.6]$
4W	$T[3,5,10]$	$U[20,50]$	$U[20,100]$	$U[28,38]$	$T[0,.3,.5]$	$T[0,.4,.7]$
5D	$T[3,9,30]$	$T[40,50,90]$	$U[40,100]$	$U[32,38]$	$T[0,.2,.4]$	$T[0,.3,.5]$

For all polygons, q_0: $U[6,12]$
C_r (Natural): $H[4,5,80,10,5]$ (or $H[7,5,20,20,20,20,10,5]$; see fig. 6.3)
C_r (Clearcut): $H[4,5,40,45,10]$ (see fig. 6.3)
γ_d: $N[95,5]$
w: $U[10,25]$
G_s: 2.4

Table 6.2—Dark 3 Level I results

Polygon	Natural state		Clearcut state	
	P_f	Hazard[1]	P_f	Hazard[1]
1D	0.005–0.010	VL	0.073–0.085	L to M
1M	.008– .013	VL	.091– .119	M
2D	.025– .040	VL to L	.161– .174	H
2M	.029– .043	VL to L	.201– .223	H
3M	.000– .000	VL	.000– .002	VL
4W	.000– .000	VL	.000– .002	VL
5D	.014– .024	VL	.176– .215	H

[1]Relative hazard based on experience of Gifford Pinchot National Forest geotechnical group:

0–0.029 = Very low (VL)
0.030–0.079 = Low (L)
0.080–0.159 = Moderate (M)
0.160–0.249 = High (H)
0.250+ = Very high (VH)

Table 6.3—Summary of potentially unstable slopes affected by timber harvest

	Acres affected		
	Alt. 1	Alt. 2	Alt. 3
Low hazard	16.3	13.7	11.0
Moderate hazard	0.0	0.0	0.0
High hazard	4.5	0.0	0.0

locations when a change in conditions was perceived. Jones recognized that depth measured to "refusal" using a hand auger may not necessarily be the depth to bedrock, as cobbles and boulders also can cause refusal. Therefore, the maximum depth used in the input distributions was somewhat greater than actually measured in the field. The soil type was finer textured (SP–SM) than was predicted by the GRC maps, with slightly plastic fines, and was easily excavated by hand (D_r of 25 to 45 percent). Shear strength and unit weight values for this different soil type were again estimated from table 5.4 and figure 5.11 of this manual. Several springs were observed in areas that were assumed to be dry in the Level I analysis, although the slopes were relatively dry overall. Therefore, distributions were developed to describe the observed conditions, rather than using the catalog of distributions developed by Wooten (1988). The distributions used for each polygon are given in table 6.4.

6.6 Level II Results

Table 6.5 gives the probabilities of failure and relative landslide hazard for each polygon. The more detailed Level II analysis using the LISA program indicates that a large portion of harvest unit 7 has a very low to low probability of failure even after timber harvest, primarily because of the gentle slopes. However, approximately 4.7 acres lie in moderate landslide hazard ground with localized failure impact, and 3.9 acres lie in high landslide hazard ground with a high likelihood of sediment entering Summit Prairie Creek should a failure occur.

Based on the Level II analysis, the District modified the unit boundary to omit the 3.9 acres having high landslide hazard. In addition, because of the observed indications of instability on the fill slope of road 2325 through the unit, Jones (1990) recommended that if timber sale alternative 1 was selected as the preferred alternative, further Level II analysis using the SARA program should be performed on the existing road and on any proposed new construction in harvest unit 7 to determine the need for further subsurface investigation, and stability analysis and design (Level III).

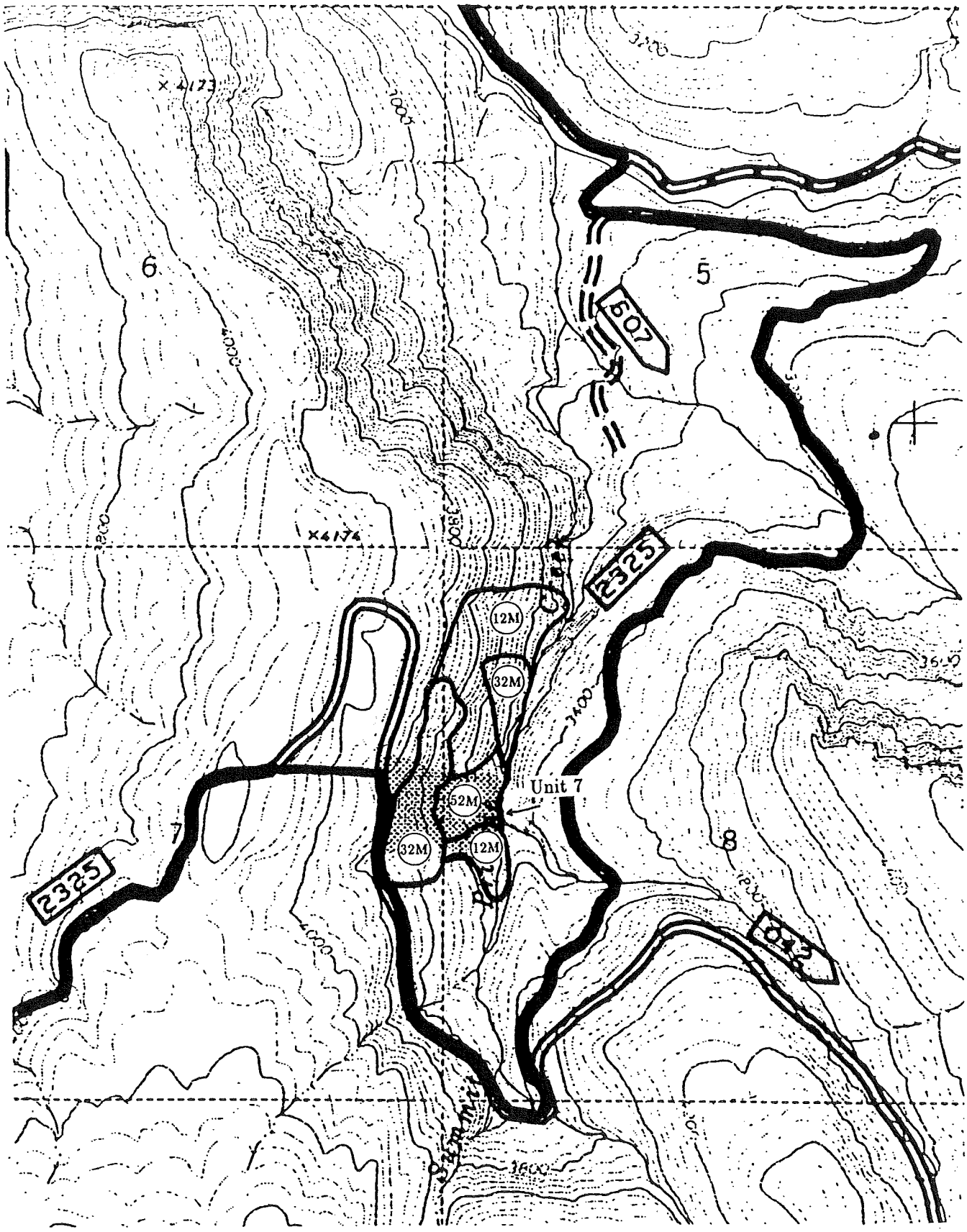

Figure 6.4—Level II analysis polygons.

Table 6.4—Distributions used in the Dark 3 Level II analysis

Polygon	D	α
12M	$T[2, 3.5, 5]$	$T[60, 70, 85]$
32M	$T[2, 3.5, 5]$	$T[65, 75, 95]$
52M	$T[2, 4, 6]$	$T[35, 55, 65]$

For all polygons,

q_0:	$U[6, 12]$			
C_r (Natural):	$H[4, 5, 80, 10, 5]$ (see fig. 6.3)			
C_r (Clearcut):	$H[4, 5, 40, 45, 10]$			
γ_d:	$N[95, 5]$			
w:	$U[10, 25]$			
G_s:	2.4			
C'_s:	$U[20, 75]$			
ϕ':	$B[28, 36, 2, 2]$			
D_w/D (Natural):	Histogram	Min	Max	%
		0.0	0.1	15
		.1	.2	40
		.2	.3	20
		.3	.4	15
		.4	.5	5
		.5	.6	1
		.6	.7	1
		.7	.8	1
		.8	.9	1
		.9	1.0	1
D_w/D (Clearcut):	Histogram	Min	Max	%
		0.0	0.1	5
		.1	.2	10
		.2	.3	20
		.3	.4	40
		.4	.5	15
		.5	.6	6
		.6	.7	1
		.7	.8	1
		.8	.9	1
		.9	1.0	1

Table 6.5—Dark 3 Level II results

	Natural state		Clearcut state	
Polygon	P_f	Hazard[1]	P_f	Hazard[1]
12M	0.019–0.025	VL	0.117–0.125	M
32M	.026– .039	VL to L	.210– .244	H
52M	.001– .004	VL	.009– .014	VL

[1]Relative hazard based on experience of Gifford Pinchot National Forest geotechnical group:

0–0.029	= Very low (VL)
0.030–0.079	= Low (L)
0.080–0.159	= Moderate (M)
0.160–0.249	= High (H)
0.250+	= Very high (VH)